Spectrum Allocation With Adaptive Sub-Band Bandwidth for Terahertz Communication Systems

Akram Shafie, *Graduate Student Member, IEEE*, Nan Yang, *Senior Member, IEEE*, Sheeraz A. Alvi, *Member, IEEE*, Chong Han, *Member, IEEE*, Salman Durrani, *Senior Member, IEEE*, and Josep Miquel Jornet, *Senior Member, IEEE*

***Abstract*— We study spectrum allocation for terahertz (THz) band communication (THzCom) systems, while considering the frequency and distance-dependent nature of THz channels. Different from existing studies, we explore multi-band-based spectrum allocation with adaptive sub-band bandwidth (ASB) by allowing the spectrum of interest to be divided into sub-bands with unequal bandwidths. Also, we investigate the impact of sub-band assignment on multi-connectivity (MC) enabled THzCom systems, where users associate and communicate with multiple access points simultaneously. We formulate resource allocation problems, with the primary focus on spectrum allocation, to determine sub-band assignment, sub-band bandwidth, and optimal transmit power. Thereafter, we propose reasonable approximations and transformations, and develop iterative algorithms based on the successive convex approximation technique to analytically solve the formulated problems. Aided by numerical results, we show that by enabling and optimizing ASB, significantly higher throughput can be achieved as compared to adopting equal sub-band bandwidth, and this throughput gain is most profound when the power budget constraint is more stringent. We also show that our sub-band assignment strategy in MC-enabled THzCom systems outperforms the state-of-the-art sub-band assignment strategies and the performance gain is most profound when the spectrum with the lowest average molecular absorption coefficient is selected during spectrum allocation.**

***Index Terms*— Terahertz communication, spectrum allocation, multi-connectivity, adaptive bandwidth.**

I. Introduction

THE scarcity of spectral resources in contemporary wireless communication systems to meet the unprecedented increase in futuristic wireless data traffic has advocated the investigation of suitable regimes in the electromagnetic spectrum for the sixth-generation (6G) and beyond era [1]. Against this backdrop, the ultra-wide terahertz (THz) band ranging from 0.1 to 10 THz has recently attracted considerable attention from the wireless communication research community [2]. The huge available bandwidths in the order of tens up to a hundred gigahertz (GHz) offer enormous potential to support emerging wireless applications that demand an explosive amount of data, such as holographic telepresence, augmented reality, virtual reality, and wireless backhaul. Built on the major progresses in THz band channel modeling and standardization efforts over the past decade, it is anticipated that indoor THz band communication (THzCom) systems will be brought to reality in the near future.

The exploration of novel and efficient spectrum allocation strategies is of paramount significance to harness the potentials of the THz band [3], [4]. When such strategies are to be devised, the unique characteristics of the THz band pose new and pressing challenges that have never been seen at lower frequencies [5]. Specifically, in addition to the severe spreading loss and the high channel sparsity, the THz band is characterized by the unique molecular absorption loss which is frequency and distance-dependent. On one hand, the molecular absorption loss divides the entire THz band into multiple ultra-wide THz transmission windows (TWs). On the other hand, it introduces drastically varying path loss even within a specific THz TW and this variation increases further as the transmission distance increases. In addition to these, limited advancements in THz band digital processors, frequency synchronizers, and transceivers make it very challenging to apply the complex spectrum reuse and multiplexing strategies that are suggested for sub-6 GHz and mmWave systems into the THz band [6]. Thus, the design of novel, low-complexity, and efficient spectrum allocation strategies is of utmost importance to develop ready-to-use THzCom systems.

A. Related Studies and Motivation

In the literature, two types of carrier-based spectrum allocation schmes have been studied for micro- and macro-scale

Manuscript received August 5, 2021; revised November 9, 2021 and December 21, 2021; accepted December 22, 2021. Date of publication December 31, 2021; date of current version February 17, 2022. The associate editor coordinating the review of this article and approving it for publication was J. A. Zhang. *(Corresponding author: Nan Yang.)*

Akram Shafie, Nan Yang, Sheeraz A. Alvi, and Salman Durrani are with the School of Engineering, The Australian National University, Canberra, ACT 2601, Australia (e-mail: akram.shafie@anu.edu.au; nan.yang@anu.edu.au; sheeraz.alvi@anu.edu.au; salman.durrani@anu.edu.au).

Chong Han is with the UM-SJTU Joint Institute, Shanghai Jiao Tong University, Shanghai 200240, China (e-mail: chong.han@sjtu.edu.cn).

Josep Miquel Jornet is with the Department of Electrical and Computer Engineering, Northeastern University, Boston, MA 02120 USA (e-mail: jmjornet@northeastern.edu).

Color versions of one or more figures in this article are available at https://doi.org/10.1109/TCOMM.2021.3139887.

Digital Object Identifier 10.1109/TCOMM.2021.3139887

multiuser THzCom systems, namely, multi-TW-based spectrum allocation and multi-band-based spectrum allocation. In the multi-TW-based spectrum allocation scheme, individual TWs are fully allocated to separate high-speed communications links while exploring wideband signals that have bandwidths equal to those of TWs [7], [8]. When this scheme is adopted in multiuser THzCom systems, the same spectrum needs to be shared among multiple users, since the number of available TWs within the entire THz band is limited [8]. This necessitates the exploration of spatial and temporal multiplexing strategies [8]. In addition, broadening and channel squint effect mitigation techniques, as well as efficient beamforming and medium access control (MAC) protocols, need to be designed to overcome interference. In the multi-band-based spectrum allocation scheme, the spectrum of interest is divided into a set of non-overlapping sub-bands that have a relatively small bandwidth, and then the sub-bands are utilized to satisfy the service demands of single or multiple users in the system [9], [10]. This scheme efficiently allocates spectral resources when there is high molecular absorption loss variation among the links in multiuser systems. Thus, this scheme has been widely explored for micro- and macro-scale multiuser THzCom applications. In this work, we focus on multi-band-based spectrum allocation for multiuser THzCom systems.

The first study on multi-band-based spectrum allocation was presented in [9] and the impacts of distance-varying usable bandwidth and different types of interference on multi-band-based spectrum allocation were discussed. Moreover, a distance-aware multi-carrier (DAMC) based sub-band assignment strategy for multi-band-based spectrum allocation was proposed in [10] to improve the throughput fairness among users in multiuser THzCom systems. Particularly, [10] proposed to assign the sub-bands that exist at the edges of the THz TW to the links with longer distances and the sub-bands that exist in the center region of the THz TW to the links with shorter distances, in order to take advantage of the frequency and distance-dependent nature of THz channels. Adopting DAMC-based spectrum allocation, resource allocation problems in non-orthogonal multiple access (NOMA) assisted THzCom systems and THz band backhaul networks were discussed in [11] and [12], respectively. In other studies, efficient sub-band assignment and transmit power algorithms based on the alternative direction method and K-means clustering were developed in [13] and [14], respectively, for NOMA-assisted THzCom systems.

Note that all the previous studies on multi-band-based spectrum allocation, i.e., [9]–[14], considered equal sub-band bandwidth (ESB), where the spectrum of interest is divided into sub-bands with equal bandwidth. However, it would be beneficial to explore spectrum allocation with adaptive sub-band bandwidth (ASB) to improve the spectral efficiency, by allowing the spectrum of interest to be divided into sub-bands with unequal bandwidths. Specifically, given that the molecular absorption loss varies considerably within THz TWs, the molecular absorption loss variation among the sub-bands would be very high when ESB is considered [9], [10]. The impact of this high variation may possibly be mitigated by adaptively adjusting the sub-band bandwidths, which leads to an overall improvement in the throughput performance. This is one of the motivations of this work. We clarify that the studies in [7], [8] considered variable bandwidths for THzCom systems. However, we note that [7], [8] explored the multi-TW-based spectrum allocation scheme. Considering variable bandwidth in this scheme, the bandwidths of communication links vary according to the variation of the usable bandwidth of THz TWs. This is different from the ASB principle in our multi-band-based spectrum allocation.

A key factor in THz band spectrum allocation is the impact of several 6G-enabling technologies, such as multi-connectivity (MC) and intelligent reflective surfaces (IRSs), which have been envisioned to be integrated into THzCom systems [3], [15], [16]. In this work, we focus on an MC-enabled THzCom system. MC allows users to associate and communicate with multiple access points (APs) simultaneously[1] [17]–[19], thereby enabling to overcome the performance degradation caused by the high vulnerability of THz signals towards blockages. With careful design, intra-band or inter-band MC strategies can be utilized to enhance the reliability and/or throughput of THzCom systems, depending on the application scenario. Here, intra-band MC refers to the utilization of one or more spectra in the THz band for association and communications [7], [20], while inter-band MC (or multiple radio access technology) refers to the utilization of spectra in both the THz band and the sub-6 GHz and/or mmWave [21], [22]. In this work, we focus on intra-band MC due to its ability to support high data rate transmission even when the primary associated link is blocked by blockers.

Spectrum allocation in an intra-band MC-enabled THzCom system was discussed in [7]. However, we note that [7] considered multi-TW-based spectrum allocation for a single user and its primary focus was on analyzing the impact of different types of MC strategies. Moreover, the resource allocation in an intra-band MC-enabled multiuser THzCom system was discussed in [20]. However, the impacts of blockages and spectrum allocation with ASB were not considered in [20]. Furthermore, it is noted that the previous studies on multi-band-based spectrum allocation in [9]–[14] did not consider the impacts of blockages, nor MC strategies. Thus, there is a need to investigate multi-band-based spectrum allocation with ASB for MC-enabled multiuser THzCom systems.

B. Our Contributions

In this work, we study spectrum allocation for intra-band MC-enabled multiuser THzCom systems, when users associate and communicate with multiple APs simultaneously. Specifically, we focus on multi-band-based spectrum allocation under the consideration that the associated links in the system are served by separate sub-bands. The main contributions of this work are summarized as follows:

[1]We clarify that several terminologies such as multi-connectivity, cooperative transmission, joint transmission, concurrent transmission, and coexisting communication, have been used in the literature to denote simultaneous association and communication of users with multiple APs [17]–[19]. However, following [17], [18], we use the term multi-connectivity in this work.

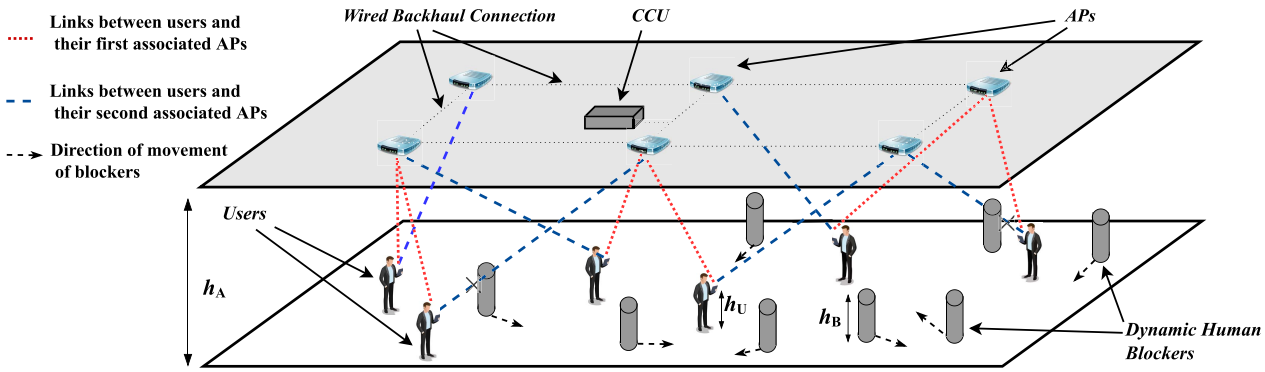

Fig. 1. Illustration of the considered 3D MC-enabled multiuser THzCom system where 6 stationary users associate with 6 fixed APs with the MC order of 2, in the presence of dynamic blockers.

- We propose multi-band-based spectrum allocation with ASB to improve the spectral efficiency and study the impact of sub-band assignment on MC-enabled multiuser THzCom systems. To this end, we formulate a generalized resource allocation problem with the objective of maximizing the throughput of the MC-enabled multiuser THzCom system, while primarily focusing on spectrum allocation. This problem consists of sub-band assignment, user association identification, sub-band bandwidth allocation, and power control. Although the generalized resource allocation problem can significantly improve the performance of the considered THzCom system when the spectrum of interest exists anywhere within a THz TW, we find that it is extremely difficult, if not impossible, to analytically solve it by using traditional optimization theory techniques. Due to this, we simplify some of the constraints in the generalized resource allocation problem and obtain two modified problems that also correspond to realistic scenarios of the considered THzCom system.
- We formulate the first modified problem, which is the resource allocation with ESB, while considering that the spectrum of interest is divided into sub-bands with equal bandwidths. The novelty of the resource allocation with ESB lies in the consideration of sub-band assignment in MC-enabled multiuser THzCom systems, while the previous relevant studies on THz band spectrum allocation have considered DAMC-based sub-band assignment, the optimality of which for MC-enabled multiuser THzCom systems needs to be validated. We also formulate the second modified problem, which is the resource allocation with ASB in either a positive absorption coefficient slope region (PACSR) or a negative absorption coefficient slope region (NACSR), while considering that the spectrum of interest fully exists in either a PACSR or an NACSR of the THz band. We define PACSRs and NACSRs as the regions with the increasing and decreasing absorption coefficient, respectively, within the THz TWs. The novelty of the resource allocation with ASB in a PACSR/NACSR lies in the consideration of multi-band-based spectrum allocation with ASB, while, to the best of our knowledge, recent studies on multi-band-based spectrum allocation for THzCom systems have only considered ESB.
- To analytically solve the resource allocation with ESB, which is a mixed-integer nonlinear problem, we introduce transformations and propose an iterative algorithm based on the successive convex approximation (SCA) technique. Also, we propose reasonable approximations and transformations to the resource allocation with ASB in a PACSR/NACSR to arrive at an approximate convex problem. Thereafter, we develop an iterative algorithm based on the SCA technique to solve the approximate convex problem.
- Aided by numerical results, we show that the proposed resource allocation with ESB outperforms the DAMC-based spectrum allocation in MC-enabled multiuser THzCom systems. The performance gain is most profound when the spectrum with the lowest average molecular absorption loss within the THz TW is selected during spectrum allocation and when the number of APs with which each user associates is high. Our results also show that the proposed resource allocation with ASB in a PACSR/NACSR achieves a significantly higher throughput performance (between 13 % and 33 %) compared to the spectrum allocation strategies that consider ESB, due to its enhanced ASB capability. The performance gain is most profound when the power budget constraint is more stringent and when the upper bound on sub-band bandwidth is very high.

II. System Model

A. System Deployment

In this work, we consider a cell free architecture based three-dimensional (3D) indoor THzCom system, as depicted in Fig. 1, where J APs cooperatively support the uplink of I stationary users which demand high data rates. We consider that APs are mounted on the ceiling of the indoor environment; thus are modeled as having the same fixed height of h_{A}. We denote $\mathcal{J} = \{1, 2, \cdots, j, \cdots, J\}$ as the set of these APs and assume that their location follows a particular layout, e.g., the layout corresponding to the indoor environment

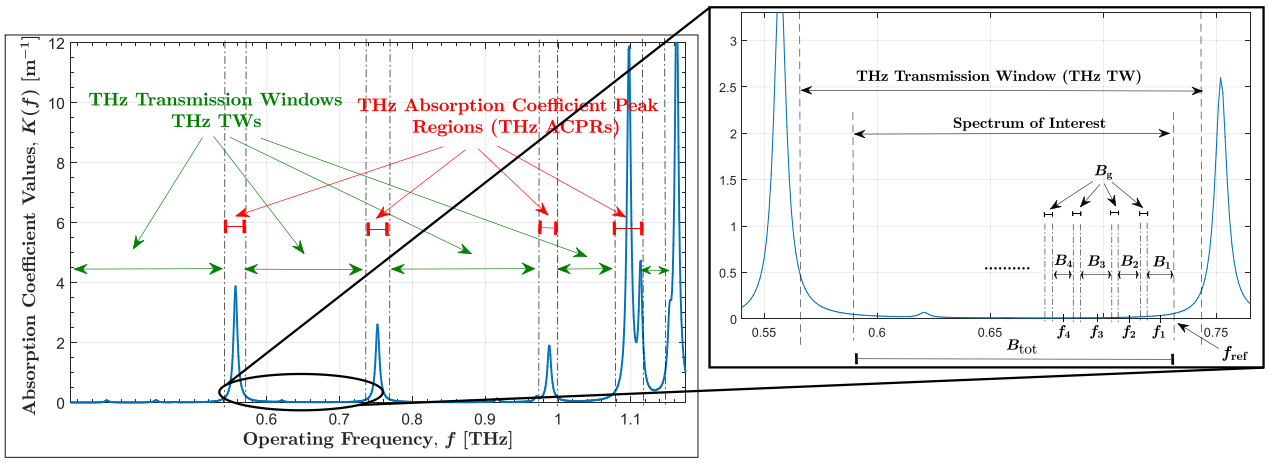

Fig. 2. Illustration of THz transmission windows, THz absorption coefficient peak regions, and the arrangement of sub-bands.

specified in the 3GPP standard [23]. We also consider that the users are distributed uniformly in the indoor environment. We denote $\mathcal{I} = \{1, 2, \cdots, i, \cdots, I\}$ as the set of the users and assume them to be of fixed height h_{U}. We denote r_{ij} and $d_{ij} = \sqrt{(h_{\mathrm{A}} - h_{\mathrm{U}})^2 + r_{ij}^2}$ as the horizontal and 3D distances of the link between the ith user and the jth AP, respectively [24].

The extremely short wavelengths of THz signals make the THz signal propagation to be highly vulnerable to blockages [5], [24]. In our system, we consider moving humans act as potential impenetrable blockers. These blockers are modeled as cylinders with the radius of r_{B} and height of h_{B} and their location follows a Poisson point process (PPP) with the density of λ_{B} [25]. We assume that the mobility of blockers follows the random directional model with constant moving speed of v_{B} [26], [27]. For the sake of practicality, we assume that $h_{\mathrm{A}} > h_{\mathrm{B}} > h_{\mathrm{U}}$ in the considered system.

We assume that users are enabled with the MC strategy of order N to overcome the performance degradation caused by blockages [7], [17]–[19], [27]. Under the MC strategy of order N, each user associates and communicates with N APs, out of the possible J APs in the system, simultaneously for user session continuity ($N \leqslant J$) [17]–[19]. We also assume that all APs are connected to a central control unit (CCU) via wired backhaul connection.

B. THz Spectrum

The intermittent molecular absorption loss peaks, that are observed throughout the THz band at different frequencies, divide the entire THz band into THz absorption coefficient peak regions (ACPRs) and ultra-wideband THz transmission windows (TWs), as shown in Fig. 2 [5]. It is envisioned that THz TWs, rather than THz ACPRs, can be utilized for applications that demand ultra-high data rates, since molecular absorption loss is relatively low in THz TWs, but very high in THz ACPRs [28]. Considering this, we focus on the allocation of the spectrum that exist within THz TWs in this work.

As mentioned in Section I, in this work we focus on multi-band-based spectrum allocation with ASB. Thus, we consider that the spectrum of interest is divided into S sub-bands with unequal bandwidths, as shown in Fig. 2. Also, we consider that these sub-bands are separated by guard bands that are of fixed bandwidth [9], [10], [29]. We denote $\mathcal{S} = \{1, 2, \cdots, s, \cdots, S\}$ as the set of the sub-bands and further denote $\mathcal{F}_{\mathcal{S}} = \{f_1, f_2, \cdots, f_s, \cdots, f_S\}$ and $\mathcal{B}_{\mathcal{S}} = \{B_1, B_2, \cdots, B_s, \cdots, B_S\}$ as the sets of their center frequency and bandwidth, respectively. We note that

$$0 \leqslant B_s \leqslant B_{\max}, \quad \forall s \in \mathcal{S}, \tag{1}$$

where $B_{\max}$ denotes the upper bound on the sub-band bandwidth. We then denote B_{g} as the fixed bandwidth of guard bands and B_{tot} as the total available bandwidth within the spectrum of interest. Considering this, we obtain

$$\sum_{s \in \mathcal{S}} B_s + (S-1) B_{\mathrm{g}} = B_{\mathrm{tot}}. \tag{2}$$

For notational convenience, we consider that sub-bands are labeled such that $f_1 > f_2 > \cdots > f_S$. Thus, we have

$$f_s = f_{\mathrm{ref}} - \sum_{k=1}^{s-1} (B_k + B_{\mathrm{g}}) - B_s/2, \quad \forall s \in \mathcal{S}, \tag{3}$$

where f_{ref} is the end-frequency of the spectrum of interest as shown in Fig. 2.

C. Channel Model

The signal propagation at the THz band is determined by spreading and molecular absorption losses. Considering this, the channel transfer function is obtained as [5]

$$H(f, d) = \frac{c}{4\pi f d} e^{-\frac{1}{2} K(f) d}, \tag{4}$$

where c is the speed of light, f is the frequency, d is the distance of interest, and $K(f)$ is the molecular absorption coefficient at f. In (4), $e^{-\frac{1}{2} K(f) d}$ represents the molecular absorption loss which is the result of oxygen molecules and water vapor absorbing THz signal energies for their rotational transition energies. We clarify that the values of $K(f)$ are obtained from $K(f) = \frac{p}{p_{\mathrm{STP}}} \frac{T_{\mathrm{STP}}}{T} \sum_{i,g} Q^{i,g} \sigma^{i,g}(f)$, where p_{STP}

and T_{STP} are the standard pressure and temperature, respectively, and p and T are the pressure and the temperature of the transmission environment, respectively [5]. Also, $Q^{i,g}$ and $\sigma^{i,g}(f)$ are the total number of molecules per unit volume and the absorption cross section for the isotopologue i of gas g at the frequency f, respectively, and they are obtained from the HITRAN database [30].

At the THz band, non-line-of-sight (NLoS) rays are substantially attenuated due to high reflection and scattering losses, as well as blockages. Due to these, NLoS rays are typically 15-20 dB weaker than that of line-of-sight (LoS) rays [5], [24], [31]. Hence, we ignore the impact of NLoS rays and focus only on the LoS rays of THz signals.

D. Performance Metrics of Interest

1) Non-Blockage Probability: If a blocker is moving according to the random directional model in a given area, the probability density function of the location of blockers is uniform over time. As such, the location of blockers forms PPP with the same intensity of λ_{B} at any given time instant [25], [26]. Considering this, the non-blockage probability of the link between the ith user and the jth AP can be derived as

$$p_{\text{nb}}(r_{i,j}) = \zeta e^{-\eta_{\text{B}} r_{i,j}}, \quad \forall i \in \mathcal{I}, j \in \mathcal{J}, \tag{5}$$

where $\zeta = e^{-2\lambda_{\text{B}} r_{\text{B}}^2}$ and $\eta_{\text{B}} = 2\lambda_{\text{B}} r_{\text{B}}(h_{\text{B}} - h_{\text{U}})/(h_{\text{A}} - h_{\text{U}})$ [25].

2) Throughput: We assume that a user transmits data through its associated links only when the corresponding links are not blocked by dynamic blockers, since blockers are impenetrable. We clarify that this assumption is adopted in previous relevant studies that investigated resource allocation in mmWave communication and THzCom environments where blockages exist [7], [19], [27], [32]. Considering this, the instantaneous achievable rate of the link between the ith user and the jth AP in sub-band s is obtained as

$$R_{i,j,s}(t) = \begin{cases} R^{\text{nb}}_{i,j,s}, \text{ with the probability of } p_{\text{nb}}(r_{i,j}), \\ R^{\text{b}}_{i,j,s}, \text{ with the probability of } (1 - p_{\text{nb}}(r_{i,j})), \end{cases} \tag{6}$$

where $i \in \mathcal{I}, j \in \mathcal{J}$, and $s \in \mathcal{S}$, $R^{\text{nb}}_{i,j,s}$ and $R^{\text{b}}_{i,j,s}$ are the achievable rates of the link between the ith user and the jth AP in sub-band s, when the link is not blocked and blocked by dynamic blockers, respectively, with $R^{\text{b}}_{i,j,s} = 0$. Mathematically, $R^{\text{nb}}_{i,j,s}$ is written as [5]

$$R^{\text{nb}}_{i,j,s} = B_s \varphi \log_2 \left(1 + \frac{P_{i,j,s} G_{\text{A}} G_{\text{U}} |\alpha_{i,j,s}|^2}{N_0 B_s + \Psi_{i,j,s}}\right), \tag{7}$$

where $P_{i,j,s}$ is the transmit power allocated by the ith user for the link between itself and the jth AP in sub-band s when the link is not blocked, G_{A} and G_{U} are the antenna gains at APs and users, respectively, N_0 is the noise spectral density, and $\Psi_{i,j,s}$ is the intra-band interference for the link between the ith user and the jth AP in sub-band s. Also, $|\alpha_{i,j,s}|^2$ is the path gain of the link between the ith user and the jth AP in sub-band s, and is given by

$$|\alpha_{i,j,s}|^2 = T_s \int_{f_s - \frac{B_s}{2}}^{f_s + \frac{B_s}{2}} |H(f, d_{i,j})|^2 \mathrm{d}f, \tag{8}$$

where T_s is the duration of the pulse transmitted in sub-band s [20]. Note that we assume that the frame duration, defined as the time interval between two consecutive pulses, is higher than that of the duration of a pulse [9], [33]. This is to overcome the impact of pulse broadening in the time domain which may lead to inter-symbol interference [9]. This is reflected in (7) using φ, where φ is the ratio between the pulse duration and the frame duration. Recently, inter-band interference (IBI) suppression schemes that can suppress IBI with minimal throughput degradation [34] and waveform designs that minimize power leakages to adjacent bands [33] were proposed. Due to these and the existence of guard bands between consecutive sub-bands in our spectrum allocation strategy, the impact of IBI is not considered in this work [20], [35].

We assume that all link distance values are available at the CCU [20]. Also, we consider that the CCU determines the optimal resource allocation policy to maximize a certain objective function. We note that although transceivers are fixed, the blocked/non-blocked state of links can change very frequently over time due to the dynamic nature of blockers [7], [32]. Therefore, it is challenging if resources are allocated dynamically over time based on the blocked/non-blocked state of links. Considering this, we assume that *the CCU determines the optimal resource allocation policy to maximize a certain long-term objective function.*[2] Finally, considering that the CCU synchronizes and combines the real-time data received from APs, the long-term throughput achieved by the ith user can be written as

$$R_i = \lim_{T \to \infty} \frac{1}{T} \int_0^T \sum_{j \in \mathcal{J}} \sum_{s \in \mathcal{S}} x_{i,j,s} R_{i,j,s}(t)\, \mathrm{d}t, \quad \forall i \in \mathcal{I}. \tag{9}$$

We next substitute (6) into (9) to obtain

$$\begin{aligned} R_i &= \sum_{j \in \mathcal{J}} \sum_{s \in \mathcal{S}} x_{i,j,s} \lim_{T \to \infty} \frac{1}{T} \int_0^T R_{i,j,s}(t)\, \mathrm{d}t \\ &= \sum_{j \in \mathcal{J}} \sum_{s \in \mathcal{S}} x_{i,j,s} \left(p_{\text{nb}} R^{\text{nb}}_{i,j,s} + (1 - p_{\text{nb}}(r_{i,j})) R^{\text{b}}_{i,j,s}\right) \\ &= \sum_{j \in \mathcal{J}} \sum_{s \in \mathcal{S}} x_{i,j,s} p_{\text{nb}} R^{\text{nb}}_{i,j,s}, \end{aligned} \tag{10}$$

where p_{nb} and $R^{\text{nb}}_{i,j,s}$ are given in (5) and (7), respectively, and $x_{i,j,s}$ is the user association and sub-band assignment indicator variable which will be discussed in the next section.

III. Optimal Resource Allocation

In this section, we first present the sub-band assignment strategy considered in this work. Thereafter, we present the generalized resource allocation problem. Finally, we discuss the challenges in solving the generalized resource allocation problem and discuss two modified problems which also represent two realistic considerations of the main optimization problem.

[2]We define the long-term value of a function as the average of the instantaneous values of this function over a relatively long-time duration. Specifically, the long-term value of the function Θ is given by $\Theta = \lim_{T \to \infty} \frac{1}{T} \int_0^T \Theta(t)\, \mathrm{d}t$, where $\Theta(t)$ is the instantaneous value of the function Θ at time instant t.

A. Sub-Band Assignment Strategy

The limited advancement in THz band digital processors hinders the benefits of using novel but complex spectrum reuse schemes for enhancing the spectral efficiency of THz-Com systems [10]. Fortunately, it is possible to achieve high throughput in THzCom systems even with a lower spectral efficiency since the bandwidths available at the THz band are in the order of hundreds of GHz [9]. Thus, following [9], [10], [20], we assume that the associated links in the system are served by separate sub-bands. This assumption ensures intra-band interference-free data transmission, i.e., $\Psi_{i,j,s} = 0$ in (7), thereby eliminating the hardware complexity and the signal processing overhead caused by frequency reuse in the system. Under this assumption, we set the number of sub-bands to be equal to the number of associated links in the system, i.e., $S = I \times N$.

Let us denote $x_{i,j,s}$ as the user association and sub-band assignment indicator variable, such that

$$x_{i,j,s} = \begin{cases} 1, & \text{if sub-band } s \text{ is assigned to the link} \\ & \text{between the } i\text{th user and the } j\text{th AP}, \\ 0, & \text{otherwise}, \end{cases} \tag{11}$$

where $i \in \mathcal{I}, j \in \mathcal{J}$, and $s \in \mathcal{S}$. As each user associates with N APs, we have

$$\sum_{j\in\mathcal{J}} \sum_{s\in\mathcal{S}} x_{i,j,s} = N, \quad \forall\, i \in \mathcal{I}. \tag{12}$$

Also, as each associated link in the system is assigned with one sub-band, we have

$$\sum_{s\in\mathcal{S}} x_{i,j,s} = \begin{cases} 1, & \text{if the link between the } i\text{th user and} \\ & \text{the } j\text{th AP is an associated link}, \\ 0, & \text{otherwise}, \end{cases} \tag{13}$$

where $i \in \mathcal{I}$ and $j \in \mathcal{J}$. We note that (13) can be equivalently written as

$$\sum_{s\in\mathcal{S}} x_{i,j,s} \leqslant 1, \quad \forall i \in \mathcal{I}, j \in \mathcal{J}. \tag{14}$$

Moreover, as each sub-band is assigned to one associated link, we have

$$\sum_{i\in\mathcal{I}} \sum_{j\in\mathcal{J}} x_{i,j,s} = 1, \quad \forall s \in \mathcal{S}. \tag{15}$$

We note that the frequency and distance-dependent nature of molecular absorption loss needs to be considered during user association and sub-band assignment in multiuser THzCom systems [9], [10]. Specifically, as shown in Fig. 3, on one hand, when the edge sub-bands (i.e., the sub-bands at the edges of the THz TW) are assigned to the links with different distances, the variation in molecular absorption gain is relatively high among the those links. On the other hand, when the center sub-bands (i.e., the sub-bands in the center region of the THz TW) are assigned to the links with different distances, the variation in molecular absorption gain is relatively low among the those links. Due to these reasons, we introduce a constraint function given by

$$|\alpha_{i,j,s}|^2 \geqslant x_{i,j,s} L_{\text{thr}}, \quad \forall i \in \mathcal{I}, j \in \mathcal{J}, s \in \mathcal{S}, \tag{16}$$

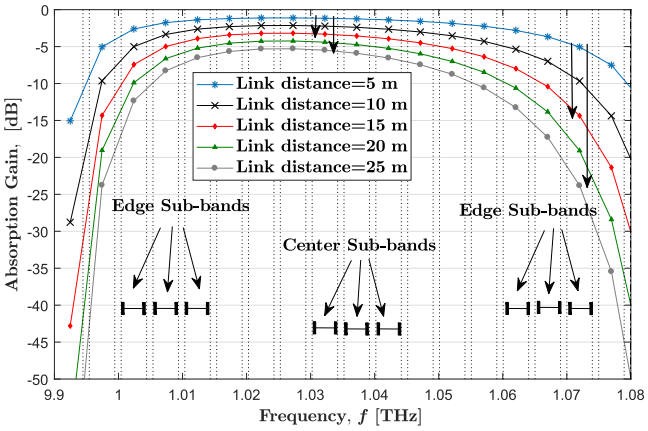

Fig. 3. Variation of absorption gain for different link distances within the first THz TW above 1 THz.

where L_{thr} is the path gain threshold imposed on the associated links. The constraint function in (16) ensures that, while the associated links with longer distances can only be assigned to center sub-bands, the associated links with shorter distances can be assigned to any sub-band within the THz TW.

B. Generalized Resource Allocation Problem

It is of utmost importance to design novel and efficient spectrum allocation strategies to harness the potential of huge available bandwidths at the THz band. With this in mind, we study the generalized uplink resource allocation problem for the considered MC-enabled multiuser THzCom system, with the primary focus on spectrum allocation. Specifically, we aim to maximize the long-term throughput under given sub-band bandwidth, power, and rate constraints. This problem consists of sub-band assignment, user association identification, sub-band bandwidth allocation, and power control. Mathematically, this problem is formulated as

$$\mathbf{P^o}: \underset{\substack{x_{i,j,s}, P_{i,j,s}, \\ B_s, \forall i,j,s}}{\text{maximize}} \quad \mathcal{E}(R_1, R_2, \cdots, R_I)$$

subject to

$$\sum_{j\in\mathcal{J}} \sum_{s\in\mathcal{S}} \zeta e^{-\eta_{\text{B}} r_{ij}} x_{i,j,s} P_{i,j,s} \leqslant P_i^{\max}, \quad \forall i \in \mathcal{I}, \tag{17a}$$

$$0 \leqslant P_{i,j,s} \leqslant P_i^{\max}, \quad \forall i \in \mathcal{I}, j \in \mathcal{J}, s \in \mathcal{S}, \tag{17b}$$

$$|\alpha_{i,j,s}|^2 \geqslant x_{i,j,s} L_{\text{thr}}, \quad \forall i \in \mathcal{I}, j \in \mathcal{J}, s \in \mathcal{S}, \tag{17c}$$

$$R_{i,j,s}^{\text{nb}} \geqslant x_{i,j,s} R_{\text{thr}}, \quad \forall i \in \mathcal{I}, j \in \mathcal{J}, s \in \mathcal{S}, \tag{17d}$$

$$\sum_{s\in\mathcal{S}} B_s + (S-1) B_{\text{g}} = B_{\text{tot}}, \tag{17e}$$

$$0 \leqslant B_s \leqslant B_{\max}, \quad \forall s \in \mathcal{S}, \tag{17f}$$

$$\sum_{j\in\mathcal{J}} \sum_{s\in\mathcal{S}} x_{i,j,s} = N, \quad \forall i \in \mathcal{I}, \tag{17g}$$

$$\sum_{s\in\mathcal{S}} x_{i,j,s} \leqslant 1, \quad \forall i \in \mathcal{I}, j \in \mathcal{J}, \tag{17h}$$

$$\sum_{i\in\mathcal{I}} \sum_{j\in\mathcal{J}} x_{i,j,s} = 1, \quad \forall s \in \mathcal{S}, \tag{17i}$$

$$\sum_{i\in\mathcal{I}}\sum_{s\in\mathcal{S}} x_{i,j,s} \leqslant M, \quad \forall j \in \mathcal{J}, \tag{17j}$$

$$x_{i,j,s} \in \{0,1\}, \quad \forall i \in \mathcal{I}, j \in \mathcal{J}, s \in \mathcal{S}. \tag{17k}$$

In $\mathbf{P^o}$, $\mathcal{E}(R_1, R_2, \cdots, R_I)$ is the objective function imposed by the considered long-term throughput maximization strategy. In this work, we aim to maximize the minimum throughput among all users, which has also been adopted by some relevant studies, e.g., [10], [20]. Therefore, $\mathcal{E}(R_1, R_2, \cdots, R_I) = \min_{i\in\mathcal{I}}\{R_i\}$. The justifications behind (17c), (17e), (17f), (17g), (17h), and (17i) are given in (16), (2), (1), (12), (14), and (15), respectively. Moreover, (17a) reflects the energy budget at each user. Specifically, recall that a user transmits data through its associated links only when the corresponding links are not blocked by dynamic blockers. Thus, we have $\sum_{j\in\mathcal{J}}\sum_{s\in\mathcal{S}} x_{i,j,s}P_{i,j,s}T_{\text{tot}}p_{\text{nb}}(r_{i,j}) \leqslant E_i(T_{\text{tot}}), \forall i \in \mathcal{I}$, where $E_i(T_{\text{tot}})$ is the energy budget of the ith user for the duration T_{tot}. This leads to (17a), where $P_i^{\max} = \frac{E_i(T_{\text{tot}})}{T_{\text{tot}}}$. Furthermore, (17d) ensures that the achievable rate of all the associated links are lower bounded by the rate threshold R_{thr}. This guarantees that a user is in coverage as long as one of its associated links is in non-blocked state. In addition, (17j) ensures that the maximum number of users with which each AP can associate is M. Finally, (17k) ensures that the user association and sub-band assignment indicator variable is binary, which reflects (11).

The novelty of our considered generalized resource allocation problem, $\mathbf{P^o}$, is two-fold. First, we propose multi-band-based spectrum allocation with ASB, while to the best of our knowledge, recent studies in THz band multi-band-based spectrum allocation have only considered ESB [9]–[14], [20]. Second, we consider sub-band assignment in MC-enabled multiuser THzCom systems under given path loss and rate constraints, while the previous relevant studies in THz band spectrum allocation have considered DAMC-based sub-band assignment, the optimality of which for MC-enabled multiuser THzCom systems needs to be validated [9]–[12]. In Section VI, we show the significance of these two considerations using numerical results.

C. Modified Problems

We note that it is challenging to solve the formulated optimization problem $\mathbf{P^o}$, due to the difficulty in obtaining the path gain, $|\alpha_{i,j,s}|^2$. On one hand, obtaining $|\alpha_{i,j,s}|^2$ as per (8) involves an integral and the limits of the integral depend on the design variables B_k, $\forall\ k \in \mathcal{S}$. On the other hand, the values of $K(f)$ for all frequencies within the spectrum of interest, i.e., $K(f)$ for $f \in F$ where $F = \{f, f_{\text{ref}} - B_{\text{tot}} \leqslant f \leqslant f_{\text{ref}}\}$, are required to obtain $|\alpha_{i,j,s}|^2$. Although $K(f)$ for $f \in F$ can be found using the methodology in [5] with the aid of HITRAN database values [30], there does not exist a tractable expression that maps f to $K(f)$. This implies that it is extremely difficult, if not impossible, to analytically solve $\mathbf{P^o}$ using the traditional optimization theory techniques. Therefore, we need to render the problem $\mathbf{P^o}$ computationally tractable. With this in mind, we simplify some of the constraints in $\mathbf{P^o}$ to obtain two modified problems and solve them using convex optimization [36]. We clarify that the two modified problems also represent two realistic scenarios of the considered THzCom system. We next discuss the two modified problems as follows:

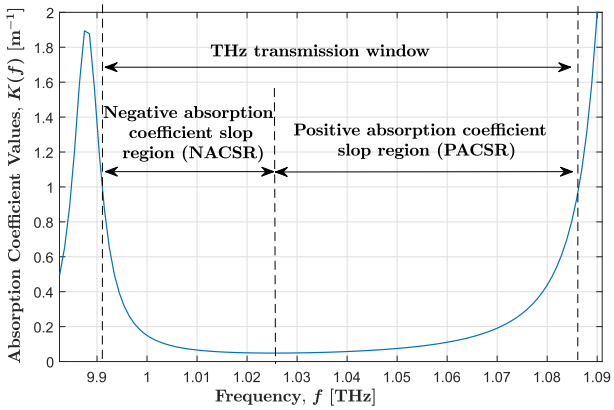

Fig. 4. Illustration of the positive and negative absorption coefficient slope regions within a THz TW.

1) Resource Allocation With ESB: In this problem, we consider that all the sub-bands are of equal bandwidth. We note that the analysis and the implementation of systems with ESB is less complex than those with ASB, since the center frequency of sub-bands is known and fixed in the former. Due to this, the spectrum arrangement with ESB has been widely considered in other emerging THz band technologies and application scenarios, e.g., NOMA for THzCom systems [11], [13], [14], THz band beamforming design [34], [37] and THz backhauling [12].

We clarify that the novelty of our resource allocation problem with ESB lies in the consideration of sub-band assignment in the considered MC-enabled multiuser THzCom system, while the previous relevant studies in THz band spectrum allocation have considered DAMC-based sub-band assignment, the optimality of which for MC-enabled multiuser THzCom systems needs to be validated. In Section IV, we formulate the resource allocation problem with ESB for the considered THzCom system. Thereafter, we solve it using convex optimization.

2) Resource Allocation With ASB in Either a PACSR or an NACSR: In this problem, we consider that the spectrum of interest fully exists either in a PACSR or an NACSR of the THz band. We note that PACSRs and NACSRs are defined as the regions within the THz TWs where $\frac{\partial K(f)}{\partial f} > 0$ and $\frac{\partial K(f)}{\partial f} < 0$, respectively, as depicted in Fig. 4. We clarify that it is reasonable to focus on the allocation of the spectrum that exists either within a PACSR or an NACSR, since the available bandwidths in each PACSR and NACSR at the THz band are in the order of tens of GHz, as shown in Table I.

We clarify that the main novelty of our resource allocation problem with ASB in a PACSR lies in the consideration of multi-band-based spectrum allocation with ASB [9]–[14], [20]. In Section V, by modifying $\mathbf{P^o}$ we first formulate resource allocation problem with ASB in a PACSR for the considered THzCom system. Thereafter, with

TABLE I
AVAILABLE BANDWIDTHS WITHIN PACSRS AND NACSRS[3] [5]

PACSR		NACSR	
Frequency Range (THz)	**Bandwidth (GHz)**	**Frequency Range (THz)**	**Bandwidth (GHz)**
$0.4934-0.5521$	58.7	$0.5620-0.6107$	48.7
$0.6734-0.7487$	78.5	$0.6207-0.6515$	30.8
$0.8702-0.9159$	45.7	$0.7559-0.8513$	95.4
$1.0250-1.0870$	62.0	$0.9905-1.025$	34.5

reasonable approximations, we transform the problem into a mixed-integer nonlinear problem. Finally, we transform the problem into a convex program utilizing additional transformations and then solve it using convex optimization. It is noted that the formulation and the solution of the resource allocation problem with ASB in an NACSR are similar to those in a PACSR. Hence, the resource allocation problem with ASB in an NACSR can be formulated and solved by directly modifying the problem formulation and the solution presented for PACSR in Section V, which is omitted in this work.

IV. RESOURCE ALLOCATION WITH ESB

In this section, we focus on the resource allocation problem with ESB for the MC-enabled multiuser THzCom system. We first formulate the problem and then solve it using convex optimization.

A. Problem Reformulation

When all the sub-bands are of equal bandwidth, the bandwidth of sub-bands, B_s, which is a design variable in $\mathbf{P^o}$, can be obtained by using (2) as $B_s=\left(F_s+\frac{1}{2}(1-2s)B_s\right)/S$, $\forall s\in\mathcal{S}$, where $F_s=f_{\text{ref}}-(s-1)B_{\text{g}}$. This helps to solve $\mathbf{P^o}$ in a tractable manner, since $|\alpha_{i,j,s}|^2$, $\forall\, i\in\mathcal{I}, j\in\mathcal{J}, s\in\mathcal{S}$, can be calculated from (8) by using the known values of B_k, where $k\in\mathcal{S}$. Considering this, the resource allocation problem with ESB for the MC-enabled multiuser THzCom system, $\mathbf{P_1^o}$, is formulated as a computationally tractable optimization program, given by

$$\mathbf{P_1^o}:\ \underset{\substack{x_{i,j,s},P_{i,j,s}\\ \forall i,j,s}}{\text{minimize}}\ \max_{i\in\mathcal{I}}\{-R_i\}\quad \text{subject to}\quad (17a)-(17d),\ (17h)-(17k). \tag{18}$$

The optimization problem $\mathbf{P_1^o}$ yields the optimal sub-band assignment and transmit power for the ESB scenario. In the next subsection, we present the solution adopted to solve $\mathbf{P_1^o}$.

B. Problem Solution

The formulated problem $\mathbf{P_1^o}$ is a mixed-integer nonlinear problem, which is non-convex in its original form [36]. In particular, the non-convexity arises from the binary constraint function (17k) since it spans a disjoint feasible solution set. Therefore, it is challenging to determine the globally optimal solution to $\mathbf{P_1^o}$ problem. To overcome this obstacle, we transform the binary variables in $\mathbf{P_1^o}$ into real variables [38]–[41]. In doing so, we rewrite the binary constraint function (17k) equivalently as the combination of two constraints, given by

$$0\leqslant x_{i,j,s}\leqslant 1,\quad \forall i\in\mathcal{I}, j\in\mathcal{J}, s\in\mathcal{S}, \tag{19}$$

and

$$\sum_{i\in\mathcal{I}}\sum_{j\in\mathcal{J}}\sum_{s\in\mathcal{S}}\left(x_{i,j,s}-x_{i,j,s}^2\right)\leqslant 0\ . \tag{20}$$

Considering (19) and (20), we transform $\mathbf{P_1^o}$ into the following equivalent problem, given by

$$\ddot{\mathbf{P}}_{\mathbf{1}}^{\mathbf{o}}:\ \underset{\substack{x_{i,j,s},P_{i,j,s}\\ \forall i,j,s}}{\text{minimize}}\ \max_{i\in\mathcal{I}}\{-R_i\}\quad \text{subject to}\quad (17a)-(17d),\ (17h)-(17j),\ (19),\ (20), \tag{21}$$

We note that in $\ddot{\mathbf{P}}_{\mathbf{1}}^{\mathbf{o}}$, although $x_{i,j,s}$ is relaxed to be real between zero and one, the constraint (20) guarantees that $x_{i,j,s}$ can only be zero or one, since $x_{i,j,s}-x_{i,j,s}^2\geq 0, \forall i\in\mathcal{I}, j\in\mathcal{J}, s\in\mathcal{S}$. Next, considering the practical computational feasibility, we relax the constraint in (20) and include it as a penalty function in the objective function. In doing so, we transform $\ddot{\mathbf{P}}_{\mathbf{1}}^{\mathbf{o}}$ into the following problem, given by

$$\bar{\mathbf{P}}_{\mathbf{1}}^{\mathbf{o}}:\ \underset{\substack{x_{i,j,s},P_{i,j,s}\\ \forall i,j,s}}{\text{minimize}}\ \max_{i\in\mathcal{I}}\{-R_i\}+\Lambda_1\sum_{i\in\mathcal{I}}\sum_{j\in\mathcal{J}}\sum_{s\in\mathcal{S}}\left(x_{i,j,s}-x_{i,j,s}^2\right)\quad \text{subject to}\quad (17a)-(17d),\ (17h)-(17j),\ (19), \tag{22}$$

where $\Lambda_1\geqslant 0$ is the constant penalty factor and $\sum_{i\in\mathcal{I}}\sum_{j\in\mathcal{J}}\sum_{s\in\mathcal{S}}\left(x_{i,j,s}-x_{i,j,s}^2\right)$ is the penalty function on the violation of the binary constraint over the objective function. We clarify that, for the optimization problem $\bar{\mathbf{P}}_{\mathbf{1}}^{\mathbf{o}}$, different optimal values can be obtained by varying Λ_1. On one hand, by setting Λ_1 extremely high, the optimal values of $\bar{\mathbf{P}}_{\mathbf{1}}^{\mathbf{o}}$ can be obtained, which would guarantee the penalty function to be extremely small, which would in turn lead to negligible violation of the binary constraint. On the other hand, by setting Λ_1 extremely low, the optimal values of $\bar{\mathbf{P}}_{\mathbf{1}}^{\mathbf{o}}$ can be obtained, which would be close to the optimal value of $\ddot{\mathbf{P}}_{\mathbf{1}}^{\mathbf{o}}$, at the cost of high violation of the binary constraint. Thus, Λ_1 must be carefully selected such that the optimal value of $\bar{\mathbf{P}}_{\mathbf{1}}^{\mathbf{o}}$ is reasonably close to the optimal value of $\ddot{\mathbf{P}}_{\mathbf{1}}^{\mathbf{o}}$, and the violation of the binary constraint is not high. Considering this, we choose Λ_1 to be sufficiently large and introduce a numerical tolerance level on the penalty function such that it is acceptable to have $\sum_{i\in\mathcal{I}}\sum_{j\in\mathcal{J}}\sum_{s\in\mathcal{S}}\left(x_{i,j,s}-x_{i,j,s}^2\right)<\epsilon$, where ϵ is a very small positive number [38]–[40].

After this manipulation, we note that the penalty function in $\bar{\mathbf{P}}_{\mathbf{1}}^{\mathbf{o}}$ is non-convex in $x_{i,j,s}$. To handle this non-convexity, we consider the Taylor approximation of the function $g(x)=x-x^2$ [41]. We observe that the Taylor approximation of $g(x)$ is convex and it provides an upper bound on $g(x)$. Considering

[3]Values are calculated for the standard atmosphere with 10% humidity, while considering that the frequencies where absorption coefficient values are less that one, belongs to THz TWs.

this, we obtain the convex upper bound on the penalty function in (22), given by

$$\sum_{i\in\mathcal{I}}\sum_{j\in\mathcal{J}}\sum_{s\in\mathcal{S}}\Big(x_{i,j,s}\big(1-2x_{i,j,s}^{(\kappa)}\big)+\big(x_{i,j,s}^{(\kappa)}\big)^2\Big) \geqslant \sum_{i\in\mathcal{I}}\sum_{j\in\mathcal{J}}\sum_{s\in\mathcal{S}}\Big(x_{i,j,s}-x_{i,j,s}^2\Big). \quad (23)$$

Finally, using (23) in (22), we transform $\mathbf{P_1^o}$ into the following approximate convex problem, given by

$$\hat{\mathbf{P}}_{\mathbf{1}}^{\mathbf{o}}: \underset{\substack{x_{i,j,s},P_{i,j,s}\\ \forall i,j,s}}{\text{minimize}} \ \max_{i\in\mathcal{I}}\{-R_i\}+\Lambda_1\sum_{i\in\mathcal{I}}\sum_{j\in\mathcal{J}}\sum_{s\in\mathcal{S}}\Big(\big(x_{i,j,s}^{(\kappa)}\big)^2 + x_{i,j,s}\big(1-2x_{i,j,s}^{(\kappa)}\big)\Big) \quad \text{subject to} \quad (17a)-(17d),\ (17h)-(17j),(19). \quad (24)$$

We clarify that $\hat{\mathbf{P}}_{\mathbf{1}}^{\mathbf{o}}$ can be solved efficiently by using standard convex problem solvers, such as CVX [42]. However, the optimal value of $\hat{\mathbf{P}}_{\mathbf{1}}^{\mathbf{o}}$ is a global upper bound on the optimal value of $\mathbf{P_1^o}$, since the upper bound on the penalty function is utilized in $\hat{\mathbf{P}}_{\mathbf{1}}^{\mathbf{o}}$. Therefore, by using the successive convex approximation (SCA) technique, we propose an iterative algorithm to tighten the upper bound obtained from solving $\hat{\mathbf{P}}_{\mathbf{1}}^{\mathbf{o}}$, which is summarized in Algorithm 1.

We finally clarify that $\hat{\mathbf{P}}_{\mathbf{1}}^{\mathbf{o}}$ is solved in each iteration of Algorithm 1 with a polynomial computational complexity. Also, there are totally $(2IJS)$ decision variables and $(3IJS+2IJ+2I+S+J)$ convex constraints in the convex problem $\hat{\mathbf{P}}_{\mathbf{1}}^{\mathbf{o}}$. Thus, solving $\hat{\mathbf{P}}_{\mathbf{1}}^{\mathbf{o}}$ requires a complexity of $\mathcal{O}\big((2IJS)^3(3IJS+2IJ+2I+S+J)\big)$ [43], [44].

Algorithm 1 Iterative Approach for Resource Allocation With ESB

1: **Initialization**: Set iteration count $\kappa=0$. Set initial point for $x_{i,j,s}^{(\kappa)}=0.5, \forall i\in\mathcal{I}, j\in\mathcal{J}, s\in\mathcal{S}$. Select a reasonably high penalty factor Λ_1 and low tolerance value ϵ.
2: **while** $\sum_{i\in\mathcal{I}}\sum_{j\in\mathcal{J}}\sum_{s\in\mathcal{S}}\Big(x_{i,j,s}\big(1-2x_{i,j,s}^{(\kappa)}\big)+\big(x_{i,j,s}^{(\kappa)}\big)^2\Big)\geqslant\epsilon$ **do**
3: Solve (24) using point $x_{i,j,s}^{(\kappa)}$, where $i\in\mathcal{I}, j\in\mathcal{J}, s\in\mathcal{S}$ and obtain solution parameters $P_{i,j,s}^*, x_{i,j,s}^*, \forall i\in\mathcal{I}, j\in\mathcal{J}, s\in\mathcal{S}$.
4: Update point $x_{i,j,s}^{(\kappa+1)}=x_{i,j,s}^*, \forall i\in\mathcal{I}, j\in\mathcal{J}, s\in\mathcal{S}$.
5: Update iteration count $\kappa=\kappa+1$.
6: **end while**

V. Resource Allocation With ASB in a PACSR

In this section, we focus on the resource allocation problem with ASB in a PACSR for the MC-enabled multiuser THzCom system. We first formulate the problem and then solve it using convex optimization.

A. Problem Reformulation

By modifying $\mathbf{P^o}$, the resource allocation problem with ASB in a PACSR for the MC-enabled multiuser THzCom system is formulated as

$$\mathbf{P_2^o}: \underset{\substack{x_{i,j,s},P_{i,j,s},\\ B_s,\forall i,j,s}}{\text{minimize}} \ \max_{i\in\mathcal{I}}\{-R_i\} \quad (25a)$$

$$\text{subject to} \quad (17a)-\ (17d),\ (17f),(17h)-(17k),$$

$$\sum_{s\in\mathcal{S}}B_s=\bar{B}_{\text{tot}}, \quad (25b)$$

where $\bar{B}_{\text{tot}}=B_{\text{tot}}-(S-1)B_{\text{g}}$. The optimization problem $\mathbf{P_2^o}$ yields the optimal sub-band assignment, sub-band bandwidth, and the transmit power for the scenario when the spectrum of interest that is to be allocated exists in a PACSR of the THz TW.

We note that the difficulties related to obtaining $|\alpha_{i,j,s}|^2$, that were mentioned in Section III-C, still exist when solving $\mathbf{P_2^o}$. To overcome this, we make two assumptions which enable us to obtain $|\alpha_{i,j,s}|^2$ using a tractable expression for the design variables B_k, $\forall\ k\in\mathcal{S}$. We next present these assumptions as follows:

First, we overcome the obstacle caused due to $|\alpha_{i,j,s}|^2$ obtained in (8) by using an integral. We observe that although the molecular absorption coefficient is frequency-dependent, its variation within sub-bands are relative small when the sub-bands have a relatively small bandwidth and sub-bands exist within THz TWs. Considering this, for tractable analysis, we represent $|\alpha_{i,j,s}|^2$ assuming that the molecular absorption coefficient remains unchanged within each sub-band. We clarify that the assumption that the molecular absorption coefficient remains unchanged within the bandwidth of interest has been adopted in previous studies such as [10], [22], [24]. This consideration enables us to obtain $|\alpha_{i,j,s}|^2$ as

$$|\alpha_{i,j,s}|^2=\frac{\varrho}{f_s^2d_{i,j}^2}e^{-K(f_s)d_{i,j}}, \quad (26)$$

where $\varrho\triangleq\big(\frac{c}{4\pi}\big)^2$.

Second, we tackle the intractability caused due to the lack of tractable expression for $K(f)$. To this end, we first obtain the values of $K(f)$ for all the values of f in the spectrum of interest using the HITRAN database and observe its variation within the spectrum of interest [30]. We notice that the variation of $K(f)$ in spectra that exist within PACSRs generally exhibits the behavior of an exponential function of f (see Fig. 4). Therefore, through curve fitting, we model $K(f)$ in the spectrum of interest using an exponential function of f, given by

$$\hat{K}(f)=e^{\sigma_1+\sigma_2 f}+\sigma_3, \quad (27)$$

where $\hat{K}(f)$ is the approximated molecular absorption coefficient at f and $\{\sigma_1,\sigma_2,\sigma_3\}$ are the model parameters obtained for the spectrum of interest. We note that the values of $\hat{K}(f)$ in other spectra that exist within PACSRs can also be modeled using exponential functions of f. However, the model parameters would differ from one spectrum to another.

We next substitute (3) and (27) into (26) to obtain

$$|\alpha_{i,j,s}|^2=\varrho\frac{e^{-\hat{K}(f_s)d_{i,j}}}{\big(f_sd_{i,j}\big)^2} =\varrho\frac{e^{-d_{i,j}[e^{\sigma_1+\sigma_2(F_s-\sum_{k\in\mathcal{S}}a_{s,k}B_k)}+\sigma_3]}}{(F_s-\sum_{k\in\mathcal{S}}a_{s,k}B_k)^2d_{i,j}^2}, \quad (28)$$

where $a_{s,k} = 1$ if $s > k$, $a_{s,k} = \frac{1}{2}$ if $s = k$, and $a_{s,k} = 0$ otherwise. Thereafter, using (28), the multiuser optimization problem for the PACSR, $\mathbf{P_2^o}$, is approximated as a mixed-integer nonlinear problem, given by

$$\bar{\mathbf{P}}_{\mathbf{2}}^{\mathbf{o}}: \underset{\substack{x_{i,j,s},P_{i,j,s},\\ B_s,\forall i,j,s}}{\text{minimize}} \ \max_{i\in\mathcal{I}}\{-R_i\} \quad \text{subject to} \quad \text{(17a)}-\text{(17d)}, \text{(17f)}, \text{(17h)}-\text{(17k)}, \text{(25b)}. \tag{29}$$

B. Problem Solution

The formulated problem $\bar{\mathbf{P}}_{\mathbf{2}}^{\mathbf{o}}$ is a non-convex problem. In particular, the non-convexity in $\bar{\mathbf{P}}_{\mathbf{2}}^{\mathbf{o}}$ arises due to three reasons. First, $R_{i,j,s}^{\text{nb}}$ that appears in the objective function in (29) and the constraint function (17d) is not differentiable at $B_s = 0$. Second, the objective function in (29) and the constraint functions (17c) and (17d) are non-convex w.r.t. the design variable B_ν, $\forall\ \nu \in \mathcal{S}$. This is due to the fact that $|\alpha_{i,j,s}|^2$ and $R_{i,j,s}^{\text{nb}}$ are not concave w.r.t. the design variable B_ν, $\forall\ \nu \in \mathcal{S}$. Third, the design variable $x_{i,j,s}$ is binary. We next tackle these challenges as follows:

We first handle the non-differentiability of $R_{i,j,s}^{\text{nb}}$ at $B_s = 0$. When the objective function is differentiable in an open domain, the Karush-Kuhn-Tucker (K.K.T.) conditions are sufficient and necessary for the optimal solution [36]. However, we note that $R_{i,j,s}^{\text{nb}}$ in $\bar{\mathbf{P}}_{\mathbf{2}}^{\mathbf{o}}$ is not differentiable at $B_s = 0$. Thus, to utilize the K.K.T. conditions to characterize the optimality of the problem in $\bar{\mathbf{P}}_{\mathbf{2}}^{\mathbf{o}}$, we consider the following approximate problem, given by

$$\bar{\mathbf{P}}_{\mathbf{2}}^{\mathbf{o}}(\delta): \underset{\substack{x_{i,j,s},P_{i,j,s},\\ B_s,\forall i,j,s}}{\text{minimize}} \ \max_{i\in\mathcal{I}}\{-R_i\} \tag{30a}$$

$$\text{subject to} \quad \text{(17a)}-\text{(17d)}, \text{(17h)}-\text{(17k)}, \text{(25b)},$$

$$\delta \leqslant B_s \leqslant B_{\max,s}, \quad \forall s \in \mathcal{S}, \tag{30b}$$

where δ is a very small positive number. We note that the optimal value of $\bar{\mathbf{P}}_{\mathbf{2}}^{\mathbf{o}}(\delta)$ converges to the optimal value of $\bar{\mathbf{P}}_{\mathbf{2}}^{\mathbf{o}}$ when $\delta \to 0^+$, i.e., $\lim_{\delta\to 0^+} \bar{\mathbf{P}}_{\mathbf{2}}^{\mathbf{o}}(\delta) = \bar{\mathbf{P}}_{\mathbf{2}}^{\mathbf{o}}$ [45].

We next handle the non-concavity of $|\alpha_{i,j,s}|^2$ and $R_{i,j,s}^{\text{nb}}$ w.r.t. the design variable B_ν, $\forall\ \nu \in \mathcal{S}$. For this purpose, we consider the following substitution for B_s, given by

$$B_s = \xi_s + \omega_s \log(\varsigma_s Z_s), \quad \forall s \in \mathcal{S}, \tag{31}$$

where $\xi_s, \omega_s, \varsigma_s > 0\ \forall\ \nu \in \mathcal{S}$. Thereafter, substituting (31) into (28) and (7), we obtain

$$|\alpha_{i,j,s}|^2 = \varrho\, \frac{e^{-d_{i,j}[e^{\sigma_1+\sigma_2(F_s-\sum_{k\in\mathcal{S}} a_{s,k}(\xi_k+\omega_k\log(\varsigma_k Z_k)))}+\sigma_3]}}{(F_s-\sum_{k\in\mathcal{S}} a_{s,k}(\xi_k+\omega_k\log(\varsigma_k Z_k)))^2 d_{i,j}^2}, \tag{32}$$

and

$$R_{i,j,s}^{\text{nb}} = (\xi_s + \omega_s \log(\varsigma_s Z_s))\varphi \times \log_2\left(1 + \frac{P_{i,j,s} G_{\text{A}} G_{\text{U}} |\alpha_{i,j,s}|^2}{N_0(\xi_s + \omega_s \log(\varsigma_s Z_s))}\right). \tag{33}$$

We observe that the expression for $|\alpha_{i,j,s}|^2$ and $R_{i,j,s}^{\text{nb}}$ in (32) and (33), respectively, are highly non-linear w.r.t. Z_ν, $\forall\ i \in \mathcal{I}, j \in \mathcal{J}, s \in \mathcal{S}, \nu \in \mathcal{S}$. However, through careful deliberation, we arrive at the following Lemma.

Lemma 1: It is found that $|\alpha_{i,j,s}|^2$ and $R_{i,j,s}^{\text{nb}}$ in (32) and (33), respectively, are concave w.r.t. Z_ν, $\forall\ i \in \mathcal{I}, j \in \mathcal{J}, s \in \mathcal{S}, \nu \in \mathcal{S}$, when $1/\omega_\nu > \bar{\omega}$, where $\bar{\omega} = \sigma_2\left(D\hat{K}(f_{\text{ref}})e^{D\sigma_3} - 1\right)$, $D > d_{\max}$, $d_{\max}$ is the maximum of link distances, i.e., $d_{\max} = \max_{i\in\mathcal{I}, j\in\mathcal{J}}\{d_{i,j}\}$.

Proof: See Appendix A. ∎

Following Lemma 1, we select ω_ν such that $1/\omega_\nu > \bar{\omega}$, $\forall\ \nu \in \mathcal{S}$, to ensure the convexity of the objective function in (29) and constraint functions (17c) and (17d) w.r.t. Z_ν. Thereafter, we transform $\bar{\mathbf{P}}_{\mathbf{2}}^{\mathbf{o}}(\delta)$ into the following equivalent problem, given by

$$\underset{\substack{x_{i,j,s},P_{i,j,s},\\ Z_s,\forall i,j,s}}{\text{minimize}} \ \max_{i\in\mathcal{I}}\{-R_i\} \tag{34a}$$

$$\text{subject to} \quad \text{(17a)} - \text{(17d)}, \text{(17h)} - \text{(17k)},$$

$$\prod_{s=1}^{S} Z_s^{\omega_s} - \prod_{s=1}^{S} \varsigma_s^{-\omega_s} e^{\bar{B}_{\text{tot}} - \sum_{s\in\mathcal{S}} \xi_s} \leqslant 0, \tag{34b}$$

$$Z_{\min,s} \leqslant Z_s \leqslant Z_{\max,s}, \quad \forall s \in \mathcal{S}, \tag{34c}$$

where $Z_{\min,s} = \frac{1}{\varsigma_s} e^{\frac{\delta-\xi_s}{\omega_s}}$ and $Z_{\max,s} = \frac{1}{\varsigma_s} e^{\frac{B_{\max}-\xi_s}{\omega_s}}$. We note that (34b) and (34c) are obtained by substituting (31) into (25b) and (30b), respectively.

We finally handle the non-convexity arising in (34) from the binary constraint function (17d). To this end, we utilize the same procedure adopted in Section IV-B, where the binary variables are transformed into real variables [39], [40]. In doing so, we approximate (34) into the following convex problem, given by

$$\hat{\mathbf{P}}_{\mathbf{2}}^{\mathbf{o}}: \underset{\substack{x_{i,j,s},P_{i,j,s},\\ Z_s,\forall i,j,s}}{\text{minimize}} \ \max_{i\in\mathcal{I}}\{-R_i\} + \Lambda_2 \sum_{i\in\mathcal{I}}\sum_{j\in\mathcal{J}}\sum_{s\in\mathcal{S}} \left(\left(x_{i,j,s}^{(\kappa)}\right)^2 x_{i,j,s}\left(1 - 2x_{i,j,s}^{(\kappa)}\right)\right)$$

$$\text{subject to } \text{(17a)} - \text{(17d)}, \text{(17h)} - \text{(17j)}, \ \text{(34c)} - \text{(34b)},$$

$$0 \leqslant x_{i,j,s} \leqslant 1, \quad \forall i \in \mathcal{I}, j \in \mathcal{J}, s \in \mathcal{S}, \tag{35}$$

where $\Lambda_2 \geqslant 0$ is the constant penalty factor. We note that, similar to the observations in Section IV, the optimal value of $\hat{\mathbf{P}}_{\mathbf{2}}^{\mathbf{o}}$ is a global upper bound on the optimal value of $\bar{\mathbf{P}}_{\mathbf{2}}^{\mathbf{o}}$. Therefore, using the SCA technique, we propose an iterative algorithm to tighten the upper bound obtained from solving $\hat{\mathbf{P}}_{\mathbf{2}}^{\mathbf{o}}$, which is summarized in Algorithm 2. Finally, we note that solving $\hat{\mathbf{P}}_{\mathbf{2}}^{\mathbf{o}}$ requires a complexity of $\mathcal{O}\big((2IJS+S)^3(3IJS+2IJ+2I+2S+J+1)\big)$ since there are $(2IJS+S)$ decision variables and $(3IJS+2IJ+2I+2S+J+1)$ convex constraints in $\hat{\mathbf{P}}_{\mathbf{2}}^{\mathbf{o}}$ [43], [44].

VI. Numerical Results

In this section, we present numerical results to illustrate the performance of the two proposed resource allocation

TABLE II
VALUE OF SYSTEM PARAMETERS USED IN SECTION VI

Parameter	Symbol	Value	Parameter	Symbol	Value
No. of users and MC order	I, N	6, 2	No. of users supported by each AP	M	3
Heights of APs and users	h_{A}, h_{U}	3.0 m, 1.3 m	Upper bound on sub-band bandwidth	$B_{\max}$	4.5 GHz
Height and radius of blockers	h_{B}, r_{B}	1.7 m, 0.3 m	Gaurd band bandwidth	B_{g}	0.75 GHz
Density of wall blockers	λ_{B}	0.2 m^{-2}	Ratio of pulse duration to frame duration[5]	φ	$1/2$
Antenna gains	G_{A}, G_{U}	25 dBi, 15 dBi	Path gain and rate thresholds per link	L_{thr}, R_{thr}	10^{-13}, 2 Gb/s
Noise spectral density	N_0	-174 dBm/Hz	Power budget per user	$P_i^{\max}$	3.2 dBm

Algorithm 2 Iterative Approach for Resource Allocation With ASB in a PACSR

1: **Initialization**: Set iteration count $\kappa = 0$. Set initial point for $x_{i,j,s}^{(\kappa)} = 0.5$, $\forall i \in \mathcal{I}, j \in \mathcal{J}, s \in \mathcal{S}$. Select a reasonably high penalty factor Λ_2 and low tolerance value ϵ.
2: **while** $\sum_{i\in\mathcal{I}}\sum_{j\in\mathcal{J}}\sum_{s\in\mathcal{S}}\left(x_{i,j,s}\left(1-2x_{i,j,s}^{(\kappa)}\right)+\left(x_{i,j,s}^{(\kappa)}\right)^2\right) \geqslant \epsilon$ **do**
3: Solve (35) using point $x_{i,j,s}^{(\kappa)}$, where $i \in \mathcal{I}, j \in \mathcal{J}, s \in \mathcal{S}$ and obtain solution parameters $P_{i,j,s}^*, x_{i,j,s}^*, Z_s^*, \forall i \in \mathcal{I}, j \in \mathcal{J}, s \in \mathcal{S}$.
4: Update point $x_{i,j,s}^{(\kappa+1)} = x_{i,j,s}^*, \forall i \in \mathcal{I}, j \in \mathcal{J}, s \in \mathcal{S}$.
5: Update iteration count $\kappa = \kappa + 1$.
6: **end while**

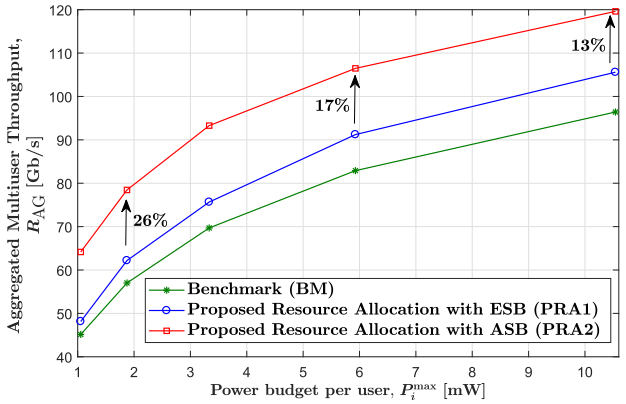

Fig. 5. Aggregated multiuser throughput versus the power budget per user.

strategies. For clarity, we denote the proposed resource allocation with ESB by PRA1 and the proposed resource allocation with ASB in a PACSR by PRA2. The numerical results are obtained by considering a rectangular indoor environment of size 20 m × 20 m. We consider that four APs are deployed symmetrically in the indoor environment in the same way as specified in the 3GPP standard [23]. Also, we consider that the 50 GHz spectrum that exists between 1.025 and 1.075 THz in the PACSR of the first THz TW above 1 THz is used to serve users.[4] We use the absorption coefficient values that are calculated for the standard atmosphere with 10% humidity [5]. The values of the rest of the parameters used for numerical results are summarized in Table II, unless specified otherwise.

For PRA2, the values of the model parameters that are utilized in (27) to approximate the absorption coefficient values in the spectrum of interest are $\sigma_1 = -90.996$, $\sigma_2 = 8.326 \times 10^{-11}$, and $\sigma_3 = 0.0452$. Moreover, in PRA2, for the substitution introduced in (31), we consider $\xi_s = 5 \times 10^9$, $\omega_s = 0.5 \times 10^9$, and $\varsigma_s = 0.001$, $\forall\, s \in \mathcal{S}$. Furthermore, following [40], [41], we consider $\Lambda_1 = 200$, $\Lambda_2 = 200$, and $\epsilon = 10^{-6}$ in Algorithm 1 and Algorithm 2. Additionally, we note that Algorithm 1 and Algorithm 2, corresponding to PRA1 and PRA2, respectively, are implemented in AMPL which is popular for modeling optimization problems [41], [46]. It is noted that to cross-check, we implement Algorithm 1 in Matlab CVX as well, and verify that the results obtained from AMPL well match those obtained from Matlab CVX.

We consider the state-of-the-art DAMC-based spectrum allocation to be the benchmark for PRA1 and denote this strategy by BM [10]. Notably, as mentioned in Section I, BM uses ESB and considers that the links with longer distances are assigned to center sub-bands and the links with shorter distances are assigned to edge sub-bands [10]. Also, we consider PRA1 to be the benchmark for PRA2 and note that while PRA1 considers spectrum allocation with ESB, PRA2 considers spectrum allocation with ASB.

In order to demonstrate the performance improvement brought by the proposed resource allocation strategies, we plot the aggregated multiuser throughput, $R_{\mathrm{AG}} = \sum_{i=1}^{N} R_i$, versus the power budget per users for BM, PRA1, and PRA2 in Fig. 5. We first observe that R_{AG} of PRA1 is higher than that of BM for different user power budget levels. This observation shows that the throughput fairness achieved by BM among associated links does not necessarily guarantee the best throughput fairness among users in an MC-enabled multiuser THzCom system. It also shows that a superior throughput fairness among the users can be achieved by utilizing PRA1. Next, as expected, we observe that PRA2 achieves a significantly higher R_{AG} compared to PRA1 (between 13 % and 26 %), due to the enhanced capabilities of PRA2 relative

[4]We clarify that it is indeed possible to utilize PRA1 when the spectrum that exists anywhere within a THz TW is to be allocated. Despite this, since PRA2 can only be employed when the spectrum of interest that is to be allocated exists in a PACSR/NACSR of the THz TW, we present numerical results for PRA1 and PRA2 in a PACSR for fair comparison.

[5]It is noted we consider that the sub-bands exist only within THz TWs, where the variation of molecular absorption loss, as well as pulse broadening, is very small. Differently, a few previous studies, e.g., [9], [33], considered that the sub-bands can also exist within ACPRs, where the variation of molecular absorption loss, as well as pulse broadening, is very high. Due to this, to avoid ISI, it is reasonable to consider $\varphi = 1/2$ in this work, when [9], [33] considered $\varphi = 1/5$.

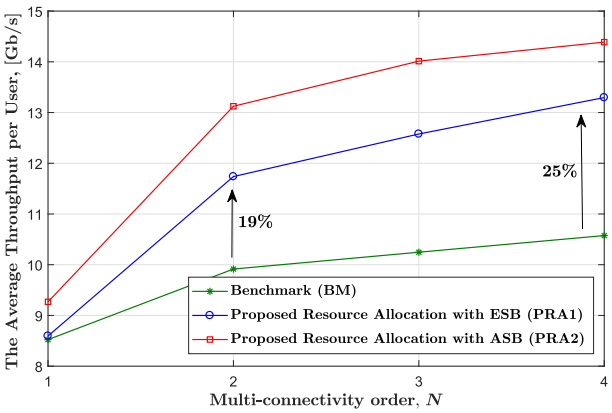

Fig. 6. The average throughput per user versus the multi-connectivity order.

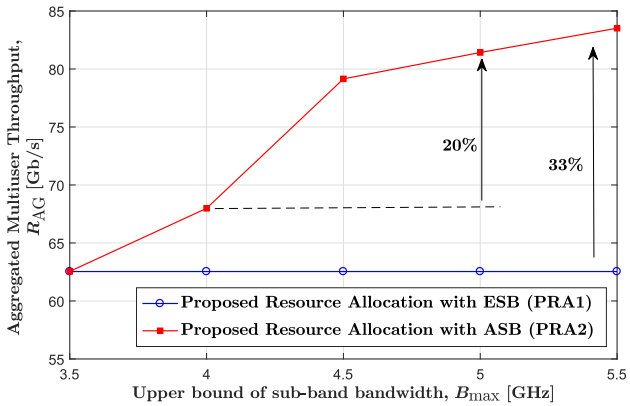

Fig. 7. Aggregated multiuser throughput versus the upper bound on the sub-band bandwidth.

to PRA1. Specifically, while PRA1 achieves a certain R_{AG} with ESB, the ASB capability of PRA2 helps to further improve R_{AG} by varying sub-band bandwidths. These two observations demonstrate the significance of the optimal sub-band assignment in MC-enabled multiuser THzCom systems and spectrum allocation with ASB, thereby demonstrating the benefits of our proposed resource allocation strategies. We further observe that R_{AG} improves for BM, PRA1, and PRA2 when the power budget increases. Interestingly, in the lower power budget regime where all strategies achieve low R_{AG}, the R_{AG} gain of PRA2 relative to PRA1 is higher, which shows that it is more beneficial to adopt ASB when the power budget constraint becomes more stringent.

In order to examine the impact of MC order on the proposed resource allocation strategies, we plot the average throughput per user versus the MC order for BM, PRA1, and PRA2 in Fig. 6. We recall that the MC order is defined as the number of APs with which the users associate and communicate simultaneously. For the sake of fairness, we keep the total number of sub-bands within the spectrum of interest unchanged. This is achieved by changing the number of users in the system when the MC order is changed. More precisely, the number of users corresponding to the MC orders of 1, 2, 3, and 4 are 12, 6, 4, and 3, respectively. We first observe that the average throughput per user increases as MC order increases. This is because, although the power budget per user remains the same as MC order increases, the available bandwidth per user increases as MC order increases, thereby improving the throughput. Second, we observe that although there exists a throughput gain for PRA1 relative to BM for the MC orders of 2, 3, and 4, the gain greatly reduces when the MC order is 1. This is due to the fact that the throughput fairness achieved by BM among associated links and the throughput fairness achieved by PRA1 among users are the same when each user associates with one AP only, i.e., MC order is 1. Third, we observe that the throughput gain for PRA1 relative to BM increases as the MC order increases from 2 to 4. This is because, as MC order increases, PRA1 gives more room to adapt the throughput among its associated links to achieve a higher throughput per user. However, as BM achieves throughput fairness among users by guaranteeing throughput fairness among links, the ability for a user to adapt throughput among its associated links does not exist when BM is employed. This leads to a low throughput improvement for BM as MC order increases, leading to a throughput gain for PRA1 relative to BM. The second and third observations jointly show that it is more beneficial to employ PRA1 when the MC order is high. Finally, we observe a steady throughput gain for PRA2 relative to PRA1, which again shows the importance of spectrum allocation with ASB.

In order to demonstrate the impact of the upper bound on the sub-band bandwidth, $B_{\max}$, which is an important constraint in PRA2, we plot R_{AG} versus $B_{\max}$ for PRA1 and PRA2 in Fig. 7. We first observe that R_{AG} of PRA2 converges to that of PRA1 when $B_{\max}$ in PRA2 is equal to the fixed sub-band bandwidth adopted in PRA1, such as $B_{\max} = 3.48$ GHz in Fig. 7. This shows the correctness of our proposed resource allocation strategies. We next observe a significant improvement in R_{AG} when $B_{\max}$ increases, e.g., a 20 % improvement in R_{AG} when $B_{\max}$ increases from 4 GHz to 5 GHz. This is expected since a larger $B_{\max}$ gives more room to exploit the ASB capability of PRA2, which improves the R_{AG} of PRA2. Here, it should be noted that the THz band amplifiers and transceivers capable of handling large bandwidth, which are required when $B_{\max}$ is higher, are in their infancy. Also, pulses occupying large bandwidths can be affected by increased pulse broadening and channel squint effects due to the frequency selectivity of molecular absorption loss within sub-bands. Thus, $B_{\max}$ of THzCom systems must be carefully selected to achieve a trade-off between improving R_{AG} performance and minimizing the complexity of software and hardware implementation.

Fig. 8 plots R_{AG} versus total bandwidth of the spectrum of interest, B_{tot}, for the proposed resource allocation strategies at different densities of human blockers, λ_{B}. Also, the spectral efficiency is plotted. We first observe that the spectral efficiency of the proposed resource allocation strategies decreases when B_{tot} increases, due to the decrease in the power density per Hz when B_{tot} increases. We next observe that R_{AG} of the proposed resource allocation strategies increases when B_{tot}

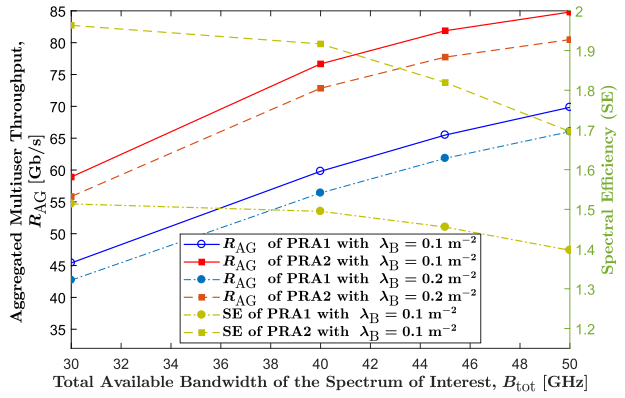

Fig. 8. Aggregated multiuser throughput and spectral efficiency versus the total available bandwidth of the spectrum of interest for different blockage densities.

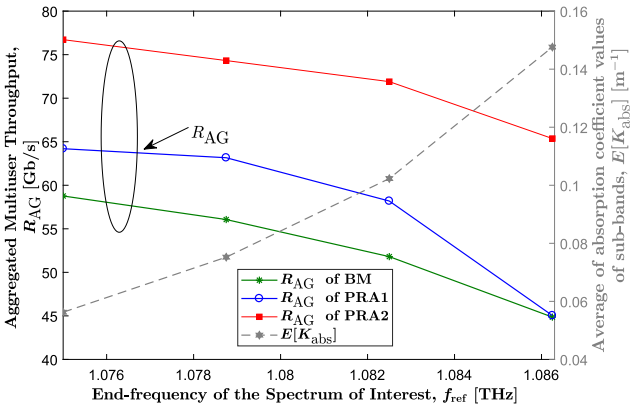

Fig. 9. Aggregated multiuser throughput versus the end-frequency of the spectrum of interest.

increases. This shows that the impact of increased availability of bandwidth for each user overwhelms the impact of decreasing spectral efficiency when B_{tot} increases. Moreover, we observe that R_{AG} of the proposed resource allocation strategies decreases with increasing λ_{B}, due to the decrease in the time during which the links are available for data transmission when λ_{B} increases. This observation emphasizes the importance of carefully selecting the system parameters, e.g., power budget, MC order, maximum sub-band bandwidth, and total available bandwidth, for achieving the desired reliability and throughput performance, depending on the density of human blockers in the indoor environment.

We finally investigate the impact of molecular absorption loss on the proposed resource allocation strategies. To this end, we consider several 50 GHz spectra within the first THz TW above 1 THz, and plot in Fig. 9 the R_{AG} for BM, PRA1, and PRA2 within these spectra versus the end-frequency of these spectra, f_{ref}. Also, the average of the absorption coefficient values of the sub-bands within these spectra, $E[K_{\mathrm{abs}}]$, is plotted. We first observe that R_{AG} for BM, PRA1, and PRA2 decreases when f_{ref} increases. This is due to the increase in $E[K_{\mathrm{abs}}]$ when f_{ref} increases, as shown in the figure, which in turn increases the molecular absorption loss in the sub-bands and reduces the reduction in R_{AG}. We next observe that the gain in R_{AG} of PRA1 relative to BM decreases when f_{ref} increases. This observation can be explained as follows. As f_{ref} increases, the number of sub-bands which have high molecular absorption loss increases. This leads to that the sub-band assignments where edge sub-bands allocated to links with shorter distances are the only sub-band assignments that can guarantee satisfying the constraint functions (17c) and (17d) in $\mathbf{P_2^o}$. This in turn leads to the convergence of R_{AG} of PRA1 to that of BM. These two observations indicate that in order to ensure improved performance, it is beneficial to select the spectrum within the THz TW that has the lowest average molecular absorption loss during spectrum allocation.

VII. Conclusion

In this work, we investigated the impacts of ASB and sub-band assignment in multi-band-based spectrum allocation on MC-enabled multiuser THzCom systems. To this end, we formulated optimization problems with the primary focus on spectrum allocation. Thereafter, we proposed reasonable approximations and transformations, and developed iterative algorithms based on the SCA technique to solve the formulated problems analytically. Aided by numerical results, we showed that by enabling ASB during spectrum allocation, the significantly higher throughput can be achieved as compared to adopting ESB and that this gain is most profound when the power budget constraint is more stringent. We also showed that the proposed sub-band assignment strategy in MC-enabled multiuser THzCom systems outperforms the state-of-the-art sub-band assignment strategy and the performance gain is most profound when the spectrum with the lowest average molecular absorption loss within the THz TW is selected during spectrum allocation.

We clarify that the solution approach proposed in this work for the spectrum allocation with ASB is only applicable when the sub-bands have a relatively small bandwidth and the spectrum of interest fully exists in either a PACSR or an NACSR of the THz band. Nevertheless, to harness the potentials of the huge available bandwidths of THz TWs, it would be more beneficial to develop a solution for the spectrum allocation with ASB when the sub-bands have a relatively high bandwidth and the spectrum of interest exists anywhere within a THz TW, which will be considered in our future work.

Appendix A
Proof of Lemma 1

We first prove the concavity of $|\alpha_{i,j,s}|^2$ w.r.t. to Z_ν, where $i \in \mathcal{I}, j \in \mathcal{J}, s \in \mathcal{S}, \nu \in \mathcal{S}$. To this end, we rearrange $|\alpha_{i,j,s}|^2$ given in (32) to obtain

$$|\alpha_s|^2 = \varrho_1 \frac{e^{-\Phi_{s,\nu} e^{-b_{s,\nu} \log(\varsigma_\nu Z_\nu)}}}{(\Omega_{s,\nu} - a_{s,\nu}\omega_\nu \log(\varsigma_\nu Z_\nu))^2}, \quad \forall s \in \mathcal{S}, \quad (36)$$

where $\varrho_1 = \varrho e^{-d\sigma_3}/d^2$, $\Phi_{s,\nu} = d(e^{\sigma_1+\sigma_2\Omega_{s,\nu}})$, $\Omega_{s,\nu} = \digamma_s - \sum_{k\in\mathcal{S}} a_{s,k}\xi_k - \sum_{k\in\mathcal{S}/\nu} \omega_k \log(\varsigma_k Z_k)$, and $b_{s,\nu} = \sigma_2 a_{s,\nu}\omega_\nu$. We note that the subscripts i and j are dropped in (36) for

brevity. Thereafter, we take the second derivative of (36) w.r.t. to Z_ν and rearrange the resulting terms to arrive at

$$\frac{\partial^2(|\alpha_s|^2)}{\partial Z_\nu^2} = \begin{cases} E_{1,1}^{s,\nu}, & \nu \leqslant s, \\ E_{1,2}^{s,\nu}, & \text{elsewhere}, \end{cases} \quad \forall s \in \mathcal{S}, \nu \in \mathcal{S}, \quad (37)$$

where $E_{1,1}^{s,\nu} = -\varrho_1 |\alpha_s|^2 b_{s,\nu}^2 \left((1+1/b_{s,\nu}) - d\hat{K}(f_s)e^{d\sigma_3}\right) \times d\hat{K}(f_s)e^{d\sigma_3}\Omega_{s,\nu}^{-2} Z_\nu^{-2}$ and $E_{1,2}^{s,\nu} = 0$. It can be shown that $E_{1,1}^{s,\nu} \leqslant 0$, $\forall\ s \in \mathcal{S}, \nu \in \mathcal{S}$, when $1/\omega_\nu > \bar{\omega}$, $\forall\ \nu \in \mathcal{S}$. Based on this, we conclude that $|\alpha_{i,j,s}|^2$ in (32) is concave w.r.t. to Z_ν when $1/\omega_\nu > \bar{\omega}$.

We next prove the concavity of $R_{i,j,s}^{\text{nb}}$ w.r.t. to Z_ν, where $i \in \mathcal{I}, j \in \mathcal{J}, s \in \mathcal{S}, \nu \in \mathcal{S}$. To this end, we rearrange $R_{i,j,s}^{\text{nb}}$ given in (33) to obtain $R_s^{\text{nb}} = B_s(Z_s)\bar{\varphi}\log(1+\Upsilon_s^\nu)$, where $B_s(Z_s) = \xi_s + \omega_s \log(\varsigma_s Z_s)$, $\bar{\varphi} = \frac{\varphi}{\log(2)}$, and $\Upsilon_s^\nu = \frac{P_s G_A G_U}{N_0 \Omega_{s,\nu}^2 B_s(Z_s)}\, e^{-\Phi_{s,\nu} e^{-b_{s,\nu}\log(\varsigma_\nu Z_\nu)}}$. Thereafter, we take the second derivative of R_s^{nb} w.r.t. to Z_ν and rearrange the resulting terms to arrive at

$$\frac{\partial^2 R_s^{\text{nb}}}{\partial Z_\nu^2} = \begin{cases} E_{2,1}^{s,\nu}, & \nu < s, \\ E_{2,2}^{s,\nu} & \nu = s, \\ E_{2,3}^{s,\nu}, & \text{elsewhere}, \end{cases} \quad \forall s \in \mathcal{S}, \nu \in \mathcal{S}, \quad (38)$$

where

$$\begin{aligned} E_{2,1}^{s,\nu} = &-Z_\nu^{-2}\left(1+\Upsilon_s^\nu\right)^{-2} B_s(Z_s) b_{s,\nu}^2 \Upsilon_s^\nu \bar{\varphi} \\ &\times\Big(\left(1+\Upsilon_s^\nu\right) \times (1+1/b_{s,\nu}) - d\ \hat{K}(f_s)e^{d\sigma_3}\Big) \\ &\times d\ \hat{K}(f_s)e^{d\sigma_3}, \end{aligned} \quad (39)$$

$E_{2,2}^{s,\nu} = T_1 + T_2 + T_3$, and $E_{2,3}^{s,\nu} = 0$ with

$$T_1 = -\frac{\bar{\varphi}\omega_s}{Z_s^2}\left(\log\left(1+\Upsilon_s^s\right) - \frac{\Upsilon_s^s}{(1+\Upsilon_s^s)}\right), \quad (40)$$

$$T_2 = -\frac{(\Upsilon_s^s)^2\bar{\varphi}\left(b_{s,s}B_s(Z_s)d\ \hat{K}(f_s)e^{d\sigma_3} - \omega_s\right)^2}{\left(1+\Upsilon_s^s\right)^2 Z_s^2 B_s(Z_s)}, \quad (41)$$

$$\begin{aligned} T_3 = &-Z_s^{-2}\left(1+\Upsilon_s^s\right)^{-1} B_s(Z_s) b_{s,s}^2 \Upsilon_s^s \bar{\varphi} \\ &\times\Big((1+1/b_{s,s}) - d\ \hat{K}(f_s)e^{d\sigma_3}\Big) d\ \hat{K}(f_s)e^{d\sigma_3}. \end{aligned} \quad (42)$$

It can be shown that $E_{2,1}^{s,\nu} < 0$ when $1/\omega_\nu > \bar{\omega}$. Also, it can be shown that $E_{2,2}^{s,\nu} < 0$ when $1/\omega_\nu > \bar{\omega}$, since $T_1 < 0$ and $T_2 < 0$, $\forall\ s \in \mathcal{S}, \nu \in \mathcal{S}$ and $T_3 < 0$ when $1/\omega_\nu > \bar{\omega}$. Based on these, we conclude that $R_{i,j,s}^{\text{nb}}$ in (33) is concave w.r.t. to Z_ν when $1/\omega_\nu > \bar{\omega}$.

REFERENCES

[1] M. Giordani *et al.*, "Toward 6G networks: Use cases and technologies," *IEEE Commun. Mag.*, vol. 58, no. 3, pp. 55–61, Dec. 2020.

[2] I. F. Akyildiz, C. Han, and S. Nie, "Combating the distance problem in the millimeter wave and terahertz frequency bands," *IEEE Commun. Mag.*, vol. 56, no. 6, pp. 102–108, Jun. 2018.

[3] M. Polese, J. M. Jornet, T. Melodia, and M. Zorzi, "Toward end-to-end, full-stack 6G terahertz networks," *IEEE Commun. Mag.*, vol. 58, no. 11, pp. 48–54, Nov. 2020.

[4] V. Petrov, T. Kurner, and I. Hosako, "IEEE 802.15.3d: First standardization efforts for sub-terahertz band communications toward 6G," *IEEE Commun. Mag.*, vol. 58, no. 11, pp. 28–33, Nov. 2020.

[5] J. M. Jornet and I. F. Akyildiz, "Channel modeling and capacity analysis for electromagnetic wireless nanonetworks in the terahertz band," *IEEE Trans. Wireless Commun.*, vol. 10, no. 10, pp. 3211–3221, Oct. 2011.

[6] C. Han, Y. Wu, Z. Chen, and X. Wang, "Terahertz communications (TeraCom): Challenges and impact on 6G wireless systems," 2019, *arXiv:1912.06040*.

[7] A. Shafie, N. Yang, and C. Han, "Multi-connectivity for indoor terahertz communication with self and dynamic blockage," in *Proc. IEEE Int. Conf. Commun. (ICC)*, Jun. 2020, pp. 1–7.

[8] Z. Hossain and J. M. Jornet, "Hierarchical bandwidth modulation for ultra-broadband terahertz communications," in *Proc. IEEE Int. Conf. Commun. (ICC)*, May 2019, pp. 1–7.

[9] C. Han, A. O. Bicen, and I. F. Akyildiz, "Multi-wideband waveform design for distance-adaptive wireless communications in the terahertz band," *IEEE Trans. Signal Process.*, vol. 64, no. 4, pp. 910–922, Feb. 2016.

[10] C. Han and I. F. Akyildiz, "Distance-aware bandwidth-adaptive resource allocation for wireless systems in the terahertz band," *IEEE Trans. THz Sci. Technol.*, vol. 6, no. 4, pp. 541–553, Jul. 2016.

[11] X. Zhang, C. Han, and X. Wang, "Joint beamforming-power-bandwidth allocation in terahertz NOMA networks," in *Proc. 16th Annu. IEEE Int. Conf. Sens., Commun., Netw. (SECON)*, Boston, MA, USA, Jun. 2019, pp. 1–9.

[12] M. Yu, A. Tang, X. Wang, and C. Han, "Joint scheduling and power allocation for 6G terahertz mesh networks," in *Proc. Int. Conf. Comput., Netw. Commun. (ICNC)*, Feb. 2020, pp. 631–635.

[13] H. Zhang, Y. Duan, K. Long, and V. C. M. Leung, "Energy efficient resource allocation in terahertz downlink NOMA systems," *IEEE Trans. Commun.*, vol. 69, no. 2, pp. 1375–1384, Feb. 2021.

[14] H. Zhang, H. Zhang, W. Liu, K. Long, J. Dong, and V. C. M. Leung, "Energy efficient user clustering and hybrid precoding for terahertz MIMO-NOMA systems," in *Proc. IEEE Int. Conf. Commun. (ICC)*, Dublin, Ireland, Jun. 2020, pp. 1–5.

[15] X. Ma *et al.*, "Joint channel estimation and data rate maximization for intelligent reflecting surface assisted terahertz MIMO communication systems," *IEEE Access*, vol. 8, pp. 99565–99581, 2020.

[16] M. F. Ozkoc, A. Koutsaftis, R. Kumar, P. Liu, and S. S. Panwar, "The impact of multi-connectivity and handover constraints on millimeter wave and terahertz cellular networks," *IEEE J. Sel. Areas Commun.*, vol. 39, no. 6, pp. 1833–1853, Jun. 2021.

[17] R. Liu, M. Lee, G. Yu, and G. Y. Li, "User association for millimeter-wave networks: A machine learning approach," *IEEE Trans. Commun.*, vol. 68, no. 7, pp. 4164–4174, Jul. 2020.

[18] M.-T. Suer, C. Thein, H. Tchouankem, and L. Wolf, "Multi-connectivity as an enabler for reliable low latency communications—An overview," *IEEE Commun. Surveys Tuts.*, vol. 22, no. 1, pp. 156–169, 1st Quart., 2020.

[19] Y. Liu, X. Fang, M. Xiao, and S. Mumtaz, "Decentralized beam pair selection in multi-beam millimeter-wave networks," *IEEE Trans. Commun.*, vol. 66, no. 6, pp. 2722–2737, Jun. 2018.

[20] A. Moldovan, P. Karunakaran, I. F. Akyildiz, and W. H. Gerstacker, "Coverage and achievable rate analysis for indoor terahertz wireless networks," in *Proc. IEEE Int. Conf. Commun. (ICC)*, May 2017, pp. 1–7.

[21] X.-W. Yao and J. M. Jornet, "TAB-MAC: Assisted beamforming MAC protocol for terahertz communication networks," *Nano Commun. Netw.*, vol. 9, pp. 36–42, Sep. 2016.

[22] J. Sayehvand and H. Tabassum, "Interference and coverage analysis in coexisting RF and dense TeraHertz wireless networks," *IEEE Wireless Commun. Lett.*, vol. 9, no. 10, pp. 1738–1742, Oct. 2020.

[23] *Study on Channel Model for Frequency Spectrum Above 6 GHz*, Standard 3GPP TR 38.900 V14.2.0, 3GPP, June 2017.

[24] A. Shafie, N. Yang, S. Durrani, X. Zhou, C. Han, and M. Juntti, "Coverage analysis for 3D terahertz communication systems," *IEEE J. Sel. Areas Commun.*, vol. 39, no. 6, pp. 1817–1832, Jun. 2021.

[25] A. Shafie, N. Yang, Z. Sun, and S. Durrani, "Coverage analysis for 3D terahertz communication systems with blockage and directional antennas," in *Proc. IEEE Int. Conf. Commun. Workshops (ICC Workshops)*, Jun. 2020, pp. 1–7.

[26] P. Nain, D. Towsley, B. Liu, and Z. Liu, "Properties of random direction models," in *Proc. IEEE INFOCOM*, Mar. 2005, pp. 1897–1907.

[27] M. Gapeyenko *et al.*, "On the degree of multi-connectivity in 5G millimeter-wave cellular urban deployments," *IEEE Trans. Veh. Technol.*, vol. 68, no. 2, pp. 1973–1978, Feb. 2019.

[28] A. Saeed, O. Gurbuz, A. O. Bicen, and M. A. Akkas, "Variable-bandwidth model and capacity analysis for aerial communications in the terahertz band," *IEEE J. Sel. Areas Commun.*, vol. 39, no. 6, pp. 1768–1784, Jun. 2021.
[29] M. Ma, X. Huang, B. Jiao, and Y. J. Guo, "Optimal orthogonal precoding for power leakage suppression in DFT-based systems," *IEEE Trans. Commun.*, vol. 59, no. 3, pp. 844–853, Mar. 2011.
[30] E. A. L. S. Rothman, "The HITRAN 2008 molecular spectroscopic database," *J. Quant. Spectrosc. Radiat. Transf.*, vol. 110, nos. 9–10, pp. 533–572, Jun. 2009.
[31] C. Han and I. F. Akyildiz, "Three-dimensional end-to-end modeling and analysis for graphene-enabled terahertz band communications," *IEEE Trans. Veh. Technol.*, vol. 66, no. 7, pp. 5626–5634, Jul. 2017.
[32] V. Petrov *et al.*, "Dynamic multi-connectivity performance in ultra-dense urban mmWave deployments," *IEEE J. Sel. Areas Commun.*, vol. 35, no. 9, pp. 2038–2055, Sep. 2017.
[33] W. Gao, Y. Chen, C. Han, and Z. Chen, "Distance-adaptive absorption peak modulation (DA-APM) for terahertz covert communications," *IEEE Trans. Wireless Commun.*, vol. 20, no. 3, pp. 2064–2077, Mar. 2021.
[34] H. Yuan, X. Wang, K. Yang, and J. An, "Hybrid precoding for cluster-based multi-carrier beam division multiple access in terahertz wireless communications," *China Commun.*, vol. 18, no. 5, pp. 81–92, May 2021.
[35] R. Liu, Q. Chen, G. Yu, and G. Y. Li, "Joint user association and resource allocation for multi-band millimeter-wave heterogeneous networks," *IEEE Trans. Commun.*, vol. 67, no. 12, pp. 8502–8516, Dec. 2019.
[36] S. Boyd and L. Vandenberghe, *Convex Optimization*. Cambridge, U.K.: Cambridge Univ. Press, 2004.
[37] H. Yuan, N. Yang, K. Yang, C. Han, and J. An, "Enabling massive connections using hybrid beamforming in terahertz micro-scale networks," in *Proc. IEEE Wireless Commun. Netw. Conf. (WCNC)*, Seoul, South Korea, Jun. 2020, pp. 1–7.
[38] E. Che, H. D. Tuan, and H. H. Nguyen, "Joint optimization of cooperative beamforming and relay assignment in multi-user wireless relay networks," *IEEE Trans. Wireless Commun.*, vol. 13, no. 10, pp. 5481–5495, Oct. 2014.
[39] D. W. K. Ng and R. Schober, "Secure and green SWIPT in distributed antenna networks with limited backhaul capacity," *IEEE Trans. Wireless Commun.*, vol. 14, no. 9, pp. 5082–5097, Sep. 2015.
[40] U. Rashid, H. D. Tuan, H. H. Kha, and H. H. Nguyen, "Joint optimization of source precoding and relay beamforming in wireless MIMO relay networks," *IEEE Trans. Commun.*, vol. 62, no. 2, pp. 488–499, Feb. 2014.
[41] S. A. Alvi, X. Zhou, S. Durrani, and D. T. Ngo, "Sequencing and scheduling for multi-user machine-type communication," *IEEE Trans. Commun.*, vol. 68, no. 4, pp. 2459–2473, Apr. 2020.
[42] M. Grant and S. Boyd. (Mar. 2014). *CVX: MATLAB Software for Disciplined Convex Programming, v2.1*. [Online]. Available: http://cvxr.com/cvx
[43] B. Soleimani and M. Sabbaghian, "Cluster-based resource allocation and user association in mmWave femtocell networks," *IEEE Trans. Commun.*, vol. 68, no. 3, pp. 1746–1759, Mar. 2020.
[44] E. Che, H. D. Tuan, and H. H. Nguyen, "Joint optimization of cooperative beamforming and relay assignment in multi-user wireless relay networks," *IEEE Trans. Wireless Commun.*, vol. 13, no. 10, pp. 5481–5495, Oct. 2014.
[45] Z. Wang, V. Aggarwal, and X. Wang, "Joint energy-bandwidth allocation in multiple broadcast channels with energy harvesting," *IEEE Trans. Commun.*, vol. 63, no. 10, pp. 3842–3855, Oct. 2015.
[46] R. Fourer, D. Gay, and B. Kernighan, "AMPL: A mathematical programming language," in *Algorithms and Model Formulations in Mathematical Programming*. (NATO ASI Series, Series F: Computer and Systems Sciences), vol. 51, S. W. Wallace, Ed. Berlin, Germany: Springer, 1989.

Akram Shafie (Graduate Student Member, IEEE) received the B.Sc. degree (Hons.) in electrical and electronic engineering from the University of Peradeniya, Sri Lanka, in 2017. He is currently pursuing the Ph.D. degree in engineering and computer science with The Australian National University (ANU), Canberra, Australia. Prior to commencing his Ph.D., he worked as a temporary Lecturer at the University of Peradeniya. His current research interests include terahertz communications, millimeter-wave communication, and machine learning in wireless communication systems.

Nan Yang (Senior Member, IEEE) received the B.S. degree in electronics from China Agricultural University in 2005 and the M.S. and Ph.D. degrees in electronic engineering from the Beijing Institute of Technology in 2007 and 2011, respectively. He has been with The Australian National University since July 2014, where he currently works as an Associate Professor at the School of Engineering. His research interests include terahertz communications, ultra-reliable low latency communications, cyber-physical security, and molecular communications. He received the IEEE ComSoc Asia–Pacific Outstanding Young Researcher Award in 2014 and the Best Paper Awards from the IEEE GLOBECOM 2016 and the IEEE VTC 2013-Spring. He also received the Top Editor Award from the *Transactions on Emerging Telecommunications Technologies*, the Exemplary Reviewer Awards from the IEEE TRANSACTIONS ON COMMUNICATIONS, IEEE WIRELESS COMMUNICATIONS LETTERS, and IEEE COMMUNICATIONS LETTERS, and the Top Reviewer Award from the IEEE TRANSACTIONS ON VEHICULAR TECHNOLOGY from 2012 to 2019. He is currently serving for the Editorial Board of the IEEE TRANSACTIONS ON MOLECULAR, BIOLOGICAL AND MULTI-SCALE COMMUNICATIONS, IEEE COMMUNICATIONS LETTERS, IEEE TRANSACTIONS ON VEHICULAR TECHNOLOGY, and *Transactions on Emerging Telecommunications Technologies*.

Sheeraz A. Alvi (Member, IEEE) received the B.S. degree in electronic engineering from the International Islamic University, Islamabad, Pakistan, in 2010, the M.S. degree in electrical engineering from the National University of Science and Technology (NUST) in 2013, and the Ph.D. degree from The Australian National University (ANU), Canberra, ACT, Australia, in 2020. From 2013 to 2016, he was a Senior Researcher with the Al-Khawarizmi Institute of Computer Science (KICS), University of Engineering and Technology (UET), Lahore, Pakistan. Prior to that, he was a Research Assistant with the School of Electrical Engineering and Computer Science (SEECS), NUST. He is currently working as a Research Fellow at the College of Engineering and Computer Science, ANU. His research interests include the Internet of Things, federated learning, and communication theory.

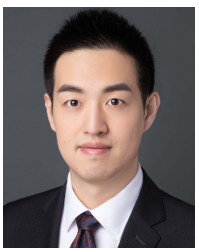

Chong Han (Member, IEEE) received the Ph.D. degree in electrical and computer engineering from the Georgia Institute of Technology, USA, in 2016. He is currently an Associate Professor with the Terahertz Wireless Communications (TWC) Laboratory, University of Michigan–Shanghai Jiao Tong University (UM-SJTU) Joint Institute, Shanghai Jiao Tong University, China. His research interests include terahertz band and millimeter-wave communication networks, and electromagnetic nanonetworks. He is a member of ACM. He was a recipient of the 2018 Elsevier *Nano Communication Networks* journal (NanoComNet) Young Investigator Award, the 2017 Shanghai Sailing Program 2017, and the 2018 Shanghai ChenGuang Program. He has been an Editor of IEEE OPEN JOURNAL OF VEHICULAR TECHNOLOGY since 2020, an Associate Editor of IEEE ACCESS since 2017, an Editor of *Nano Communication Networks* journal (Elsevier) since 2016, and a TPC chair to organize multiple IEEE and ACM conferences and workshops.

Salman Durrani (Senior Member, IEEE) received the B.Sc. degree (Hons.) in electrical engineering from the University of Engineering and Technology, Lahore, Pakistan, in 2000, and the Ph.D. degree in electrical engineering from The University of Queensland, Brisbane, QLD, Australia, in December 2004. He has been with The Australian National University, Canberra, ACT, Australia, since 2005, where he is currently an Associate Professor with the School of Electrical Engineering, College of Engineering and Computer Science. He has coauthored more than 150 publications to date in refereed international journals and conferences. His research interests include wireless information and power transfer, energy-harvesting-enabled wireless communications, drone communications, machine-to-machine and device-to-device communication, stochastic geometry modeling of finite area networks, and synchronization in communication systems. He is also a member of Engineers Australia, a Senior Fellow of IEEE, USA, and a Senior Fellow of the Higher Education Academy, U.K. He was a recipient of the 2016 IEEE ComSoc Asia–Pacific Outstanding Paper Award. He was awarded the special Commendation in the 2019 ACGR Award for Excellence in Graduate Research Supervision, the 2018 ANU VC Award for Excellence in Supervision, and the 2012 ANU VC Award for Excellence in Education. He was the Chair of the ACT Chapter of the IEEE Signal Processing and Communications Societies from 2015 to 2016. He has served as an Editor for the IEEE TRANSACTIONS ON COMMUNICATIONS from 2015 to 2020.

Josep Miquel Jornet (Senior Member, IEEE) received the B.S. degree in telecommunication engineering and the M.Sc. degree in information and communication technologies from the Universitat Politècnica de Catalunya, Barcelona, Spain, in 2008, and the Ph.D. degree in electrical and computer engineering from the Georgia Institute of Technology (Georgia Tech), Atlanta, GA, USA, in 2013. From August 2013 and August 2019, he was a Faculty with the Department of Electrical Engineering, University at Buffalo (UB), The State University of New York. Since August 2019, he has been an Associate Professor with the Department of Electrical and Computer Engineering, the Director of the Ultrabroadband Nanonetworking Laboratory, and a Faculty Member of the Institute for the Wireless Internet of Things, Northeastern University (NU), Boston, MA, USA. His research interests are in terahertz communication networks, wireless nano-bio-communication networks, and the Internet of Nano-Things. In these areas, he has coauthored more than 180 peer-reviewed scientific publications, one book, several book chapters, and has also been granted four U.S. patents. He is serving as the lead PI on multiple grants from U.S. federal agencies, including the National Science Foundation, the Air Force Office of Scientific Research, and the Air Force Research Laboratory. He was a recipient of the National Science Foundation CAREER Award and several other awards from IEEE, ACM, UB, and NU. He is also an IEEE ComSoc Distinguished Lecturer for the class of 2022–2023. Since July 2016, he has been the Editor-in-Chief of the *Nano Communication Networks* (Elsevier) journal.